SYNTHESIS OF CDTE AND PBS SEMICONDUCTOR QUANTUM DOTS AND THEIR BIOLOGICAL AND PHOTOCHEMICAL APPLICATIONS

by

XING ZHANG

Presented to the Faculty of the Graduate School of

The University of Texas at Arlington in Partial Fulfillment

of the Requirements

for the Degree of

MASTER OF SCIENCE IN PHYISCS

THE UNIVERSITY OF TEXAS AT ARLINGTON

May 2010

ACKNOWLEDGEMENTS

My research project would not have been possible without the continuous support of many people. First I want to offer my sincerest gratitude to my supervisor, Dr Wei Chen, who has support me throughout my project with this patience and knowledge. Then I want to thank everyone within our group, Marius Hossu, Yuebin Li, Lun Ma, Mingzhen Yao, Boonkuan Woo for sharing the knowledge as well as ideas throughout the research process. Without them, I would never have gone this far.

I would also like to thank Dr Ali Koymen, Dr. Samarendra Mohanty and Georgios Alexandrakis for serving as my defense committee. My special gratitude goes to Dr Qiming Zhang for his priceless suggestions on my academics as well as my career.

Dr Zdzislaw Musielak, Dr Georgios Alexandrakis and Dr Nail Fazleev and all the faculty members in UTA, thank you for sharing your knowledge with me. I really learned a lot from you.

I want to give my deepest gratitude to my family, especially to my father. He shaped my character as well as spirit when I was still a little boy, to the last moment of his life. I could not have achieved this without his guidance, and also my mother, for taking good care of my father while I was away in the US. Thank you for your understanding and the courage you have given me.

April 22, 2010

ABSTRACT

SYNTHESIS OF CDTE AND PBS SEMICONDUCTOR QUANTUM DOTS AND THEIR BIOLOGICAL AND PHOTOCHEMICAL APPLICATIONS

Xing Zhang, M.S.

The University of Texas at Arlington, 2010

Supervising Professor: Wei Chen

Semiconductor quantum dots are inorganic nanoparticles with unique photophysical properties. In particular, water soluble quantum dots which have been synthesized by colloidal chemistry in aqueous environment are highly luminescent. Their high absorption cross sections, tunable properties, narrow emission bands and effectiveness of surface functionality have stimulated the usage of these luminescent probes in various applications like biological sensors as well as imaging contrast agents. This thesis presents several aspects about the synthesis of highly luminescent water soluble, CdTe quantum dots, their near infrared counterpart $Hg_xCd_{1-x}Te$ and application such as using CdTe quantum dots for the quantitative analysis of the photosensitizer protoporphyrin IX (PPIX) while also discussing singlet oxygen detection. Finally, the synthesis of extremely crystallized PbS quantum dots will be described alongside with their application of the electrochemical assay for detection of the cancer embryonic antigen (CEA).

TABLE OF CONTENTS

LIST OF ILLUSTRATIONS

LIST OF TABLES

CHAPTER 1

INTRODUCTION

1.1 Nanoscience and Nanotechnology

In recent years nanoscience has shown itself to be one of the most exciting areas in science, with experimental developments being driven by pressing demands for new technological applications. It is a highly multidisciplinary research field and the experimental and theoretical challenges for researchers in the physical sciences are substantial. Nowadays, scientists and research scholars have been developing new kinds of nano materials which could be used for forensic science, biology, electronic technology, environmental science, computer manufacturing, sports facility production as well as food industries. In Jan 21st, 2000 Caltech, President Bill Clinton advocated nanotechnology development and raised it to the level of a federal initiative, officially referring to it as the National Nanotechnology Initiative (NNI).

But what is nanoscience and nanotechnology and why is it so important to us? Nanoscience and nanotechnology is a type of applied science, studying the ability to observe, measure, manipulate and manufacture materials at the nanometer scale. The prefix nano in the word nanometer (nm) is an SI unit of length, namely 10^{-9} or a distance of one-billionth of a meter. As a comparison, a head of a pin is about one million nanometers wide or it would take about 10 hydrogen atoms end-to-end to align in series in order to span the length of one nanometer. Because the matter it deals with is smaller than the macroscopic scale which could be seen by our naked eye, but larger than the microscopic scale of the electrons and protons and that could only been sensed by cloud chambers, it dwells in a new realm called mesoscopic scale which contains the domain of 10^{-7} to 10^{-9} nm. In other words, whenever a macroscopic device is scaled down to mesoscopic scale, it starts revealing quantum mechanical properties. While macroscopic scale could be studied by Classical Mechanics and microscopic scale could be expressed by Quantum Mechanics, mesoscopic scale is somewhere in between and our knowledge about this field is quite limited. This has stimulated the scientists to start a new territory dealing with the “bridge” which connects the macro and micro, this “bridge” being the so called nanoscience.

Why should this be emphasized that often? Because making products at the nanometer scale is and will become a big economy for many countries. By 2015, nanotechnology could be a $1 trillion

industry and meanwhile, according to National Nanotechnology Initiative, scientists will create new ways of making structural materials that will be used to build products and devices atom-by-atom and molecule-by-molecule. These nanotechnology materials are expected to bring about lighter, stronger, smarter, cheaper, cleaner, and more durable products. One of the main reasons why there is a lot more activities in producing nanotechnology products today than before is because there are now many new kinds of facilities that can handle nanomaterials including, but not limited to, transmission electron microscopy (TEM) which could directly see the atoms clusters; and atom force microscopy (AFM) which can measure, see, and manipulate nanometer-sized particles; nanoimprint lithography (NIL) which is equipped with high-precision alignment system with accuracy within 500nm and fine alignment up to 50nm; Physical Vapor Disposition (PVD) and Chemical Vapor Disposition (CVD) as well as Molecular Beam Epitaxy (MBE) systems which allow the scientists to accurately control the ingredients of the nanodevices when manufacturing them.

With more and more nanotechnologies emerging into our lives and the benefits it provided after been manufactured and become commercially available, it will also bring some ethical, legal, social and moral issues as well. Most of them are not new problems but because of nanotechnology their importance and urgency have been emphasized to a new level. From technology perspective, nanotechnology has stimulated its application in national defense and weapons, e.g. the materials with high stiffness and high strength made of carbon nanotubes, so that weapons made from these materials could hardly been identified by probes which are only suited for detection of metal based weapons. On the other hand this would bring a lot of problems for the TSA (Transportation Security Administration) to detect criminals who want to get on planes or enter security areas. Potentially, whether it is still safe to use nanotechnology in cosmetics, food and apparel industry is still under investigation. Because nanoparticles are so small, they could easily permeate into living body without being noticed, and while there is not enough knowledge about the interaction of these nanoparticles with our body organs and systems. They could be involved in cancer development or in certain kind of new diseases which could not be cured. These are all heady questions, and as time goes by, these problems would become much more serious and it is time for the public to know what “nano” really is and what else it could mean. By far not only scientists are involved in solving these problems because nanotechnology is already, intrinsically, a multidisciplinary science.

1.2 Quantum Dots

Quantum dots, the so-called nanocrystals, are nano-sized semiconductor particles composed of II-VI group or III-V main group elements. Normally, the size of the quantum dots is between 1 ~ 100 nm. Since the electrons and holes within are quantumly confined in all three spatial dimensions, the continuous bandgap structures of the bulk material would become discrete if excited to higher energy states. When the quantum dots return to their ground state, a photon of a frequency characteristic of that material is emitted. As a result, they have properties that are between those of bulk materials and those of discrete molecules. Quantum dots have so many applications in solar cells, light emitting devices, photo bio-labeling technologies because of the following reasons:

- Absorbance and emissions can be tuned with size
- Higher quantum yields
- Broad excitation window but narrow emission peaks
- Less photobleaching
- Higher extinction coefficients
- Minimal interference with each other could be avoided when used in the same assay
- Functionality possible with different bio-active agents in order to suit specific outcomes.
- More photostable when exposed to ultraviolet excitation than organic dyes. [1-3]

1.2.1 Quantum size confinement effects

Quantum confinement is the phenomenon which is the widening of the bandgap energy of the semiconductor material when its size has been shrunken to nano scale. The bandgap of a material is the energy required to create an electron and a hole with zero kinetic energy at a distance far enough apart that their Coulombic attraction could be ignored. A bound electron-hole pair, termed exciton, would be generated if one carrier approaches the other. This exciton behaves like a hydrogen atom, except that a hole, which is not a proton, forms the nucleus. We define the distance between the electron and hole to be the exciton Bohr radius (r_B). If m_e and m_h are the effective masses of electrons and holes, respectively, the exciton Bohr radius can be expressed by

$$r_B = \frac{\hbar^2 \varepsilon}{e^2}\left(\frac{1}{m_e} + \frac{1}{m_h}\right) \tag{1.1}$$

where ε, $\hbar$ and e are the dielectric constant, reduced *Planck constant* and the charge of an electron respectively[4].

If the radius (R) of a quantum dot shrinks to r_B, especially when $R<r_B$, the motion of the electrons and holes are strongly confined spatially to the dimension of the quantum dot. Consequently, the excitonic transition energy and the bandgap energy will increase, which results the blue shift of the emission of the quantum dot.

1.2.2 Radiative Relaxation

Radiative Relaxation is the spontaneous luminescence from quantum dots. It consists of several types of mechanisms: band edge or near band edge transition, defect or activator quantum states transition.

1.2.2.1 Band edge emission

The most general Radiative relaxation processes in intrinsic semiconductors and insulators are band edge and near band edge (exciton) emission. The recombination of an excited electron in the conduction band with a hole in the valence band is called band edge emission. An electron and hole pair may be bound by a few meV to form an exciton. The radiative recombination of an exciton leads to near band edge emission at energies slightly lower than the band gap. Radiative emission may also be characterized as either fluorescence or phosphorescence, depending on the path required to relax. Fluorescence exhibits short radiative relaxation lifetimes (10^{-9}~10^{-5} s) [5]. Radiative relaxation processes with lifetimes longer than 10^{-5} s are called phosphorescence.

In a typical photoluminescence (PL) process, an electron in a quantum dot is excited by absorption of an electromagnetic wave, hv, from its ground state to an excited state. Through a fast vibrational (nonradiative) process, the excited electron relaxes to its lowest energy excited vibrational state. For electronic relaxation in molecules, nanoparticles or bulk solids, the emitted photon is red shifted relative to the excitation photon energy/wavelength (i.e. *Stokes shift*) because of the presence of vibrational level in the excited state as well as the lower energy (e.g. ground) states. Both organic and inorganic luminescent quantum dots exhibit Stokes shift. In organic quantum dots, this relaxation process may be complicated by crossing from singlet to triplet excited states [5]. When intersystem crossing happens, the lifetime is long (10^{-5}~10 s) and the emission is classified as phosphorescence.

1.2.2.2 Defect emission

Radiative emission from quantum dots also comes from localized impurity and/or activator quantum states in the band gap. Defect states are called dark states when they lie inside the bands themselves. Depending on the type of defect or impurity, the state can act as a donor (has excess electrons) or an acceptor (has a deficit of electrons). Electrons or holes are attracted to these sites of deficient or excess local charge due to Coulombic attraction.

1.2.2.3 Activator emission

Luminescence generated by intentionally incorporated impurities is called extrinsic luminescence. The band structure could be perturbed by the impurities, the so-called activators, in the way of creating local quantum states that lies within the band gap. The predominant radiative mechanism in extrinsic luminescence is electron-hole recombination, which can occur via transition from conduction band to acceptor state, donor state to valance band or donor state to acceptor state.

1.2.3 Non-radiative relaxation

In the case of the transition from excited state to the ground state, quantum dot might not emit the photons. Therefore, deep level traps have a tendency to undergo nonradiative recombination by emitting phonons. This non-radiative relaxation process consists of three types: internal conversion, external conversion or Auger recombination. Internal conversion is the nonradiative recombination through crystalline and/or molecular vibrations, and is also one of the reasons for Stokes shift. External conversion is the process where non-radiative relaxation occurred at surface states, defects due to unsaturated dangling bonds etc. Auger non-radiative relaxation refers to strong carrier-to-carrier interaction, which is the process where the excess energy is transferred to another electron that is called an Anger electron instead of releasing the energy as photon or phonon.

1.2.4 Surface Passivation

As described from previous section, we already know that in order to reduce the non-radiative relaxation, one of the effective ways is to reduce the surface defects, getting rid of temporary “traps” for the electrons, holes or excitons, resulting better quantum yield for quantum dots. Therefore, in order to achieve photostable quantum dots product, capping or passivation of the surface is critical. Generally, there are two ways to accomplish this goal. One is to cap the quantum dots by organic molecules. The other is of course to cap the quantum dots by inorganic layers. In general, phosphenes, (e.g. tri-n-octyl

phosphene oxide, namely TOPO [6]) or mercaptans (-SH [7]) are the most widely used capping ligands. Organic molecules however are distorted in shape and, as a result, coverage of surface atoms with the organic capping molecules may be sterically hindered. Besides, the organic capped quantum dots are photounstable. The bonding at the interface between the capping molecules and surface atoms is generally weak, leading to the failure of passivation and creation of new surface states, especially under UV irradiation. The surface states of nanocrystals are known by sites of preferential photodegradation and luminescence quenching. Compared with organic passivated quantum dots, inorganic layer passivated quantum dots have some merits. Uniform coating could be coated on the surface of the quantum dots in order to accomplish high quantum yield. The maximum of core/shell quantum dots is also dependent upon the thickness of the shell layer. Thicker capping layers lead to formation of misfit dislocations, which are also non-radiative recombination sites which decrease the luminescence intensity. Generally, materials with wider bandgap normally play the coating role, while the materials with narrower bandgap are made to be the quantum dots core. In this way, exciton could be confined into the core region by the band offset potentials. Another factor to consider when selecting the quantum dots inorganic shell material includes whether it is hydrophobic or hydrophilic. Most inorganic core/shell quantum dots are not compatible with dispersion in water due to the hydrophobic surface property of the shell. In order to be biologically friendly, an appropriate water-compatible coating such as amorphous silica layers is crucial. For best passivation, the shell material should have a lattice parameter within 12% of the core to encourage epitaxy and minimize strain, and a thickness below the critical value that results in misfit dislocations.

1.3 Quantum Dots Synthesis Process

There are two popular ways to synthesize quantum dots: one is top-down and the other is bottom-up approach.

1.3.1 Top-down synthesis

In the top-down approaches, bulk semiconductor is thinned to form quantum dots. Several other facilities have been involved in research work like this for decades, e.g. electron beam lithography (EML), reactive-ion etching, focused ion beams and dip pen lithography. The major shortcomings with these approaches include incorporation of impurities into the quantum dots materials and structural

imperfections by patterning. In this research paper, we are not going to use this method to synthesize our quantum dots.

1.3.2 Bottom-up approach

Bottom-up approach means to synthesize the nano scale material by taking advantage of the chemistry and physics to artificially combine the atoms and molecules in a nanoparticles cluster.

1.3.2.1 Chemical methods

By careful controlling of the parameters for a single solution or mixture of solution to precipitate, nucleuses are generated and further nanoparticles growth may be achieved. Nucleation may be categorized as homogeneous, heterogeneous or secondary nucleation. Homogeneous nucleation occurs when solute atoms or molecules combine and reach a critical size without the assistance of a pre-existing solid interface. By varying factors such as temperature, electrostatic double layer thickness, stabilizers or micelle formation, concentrations of precursors, ratios of anionic to cationic species and solvent, quantum dot of the desired size, shape and composition have been produced. Some of the common synthesis processes are the famous hydrothermal synthesis process, sol-gel process, microemulsion process, hot-solution decomposition process, and microwave synthesis process to name just a few. Detailed explanation that is pertinent to the production of quantum dots used in this work will be provided further.

1.3.2.2 Physical methods

Physical methods for synthesizing quantum dots begin with steps in which layers are grown in an atom-by-atom process. For example, molecular bean epitaxy (MBE) has been used to deposit the overlayers and grow elemental, compound or alloy semiconductor manostructured materials on a heated substrate under ultra-high vacuum ($\sim 10^{-10}$ Torr) conditions. Physical vapor deposition (PVD) grows layer by condensing of solid from vapors produced by thermal evaporation or sputtering. Quantum dots can be self assembled on a thin film by chemical vapor deposition (CVD).

1.4 Quantum Dots Biological Applications

Quantum dots are small, compared with biological tissues, they are robust and very stable light emitters and they can be broadly tuned simply through size variation, making them become competitive candidates for biological applications. In the past two years, there has been development of a wide range of methods for bio-conjugating colloidal quantum dots [8-11] for cell labeling [12], cell tracking [13], *in vivo* imaging [14] and DNA detection [15, 16]. Colloidal quantum dots with a wide range of bio-

conjugation and with high quantum yields are now available commercially. Therefore neither the researchers need to synthesize the quantum dots on their own (which requires a lot of experience and a firm background on chemistry and materials science), nor do they have to become lost in the discussion concerning various parameters controlling the properties of specific type of quantum dots and their water solubility as well as bio-compatibility. Among traditional applications that have been affected by the utilization of quantum dots are fluorescence resonance energy transfer analysis, magnetic resonance imaging, cell labeling.

1.4.1 Fluorescence resonance energy transfer analysis

Fluorescence resonance energy transfer (FRET) involves the transfer of fluorescence energy from a donor particle to an acceptor particle whenever the distance between the donor and the acceptor is smaller than a critical radius, known as the Förster radius [17]. This leads to a reduction in the donor's emission and excited state lifetime, and an increase in the acceptor's emission intensity. FRET is suited to measuring changes in distance, rather than absolute distances [18], making it appropriate for measuring protein conformational changes [19], monitoring protein interactions [20] and assaying of enzyme activity [21]. Several groups have attempted to use quantum dots in FRET technologies [22], particularly when conjugated to biological molecules [23], including antibodies [11], for use in immunoassays.

1.4.2 Imaging magnetic quantum dots with magnetic resonance imaging (MRI)

Magnetic resonance imaging has been shown to be very well suited for diagnostic cancer imaging as a result of the outstanding anatomical resolution of this modality [24, 25]. The basis of molecular MRI is generally based on the assumption that antibodies, peptides, or other targeting molecules, tagged with a magnetic contrast agent, binds to the target and produces a local magnetic field perturbation that results in an increased proton relaxation rate that is detectable by magnetic resonance techniques. Magnetic quantum dots are a form of magnetic contrast agent in MRI. Para- and superparamagnetic agents such as Gd(III) and various forms of iron oxide in both molecular and nanoparticles form have been used in a broad range of MRI applications to enhance image contrast. This approach is only limited by the inherent sensitivity of MRI, and the specific pulse sequence chosen, to the presence and distribution of the magnetic contrast agent [26-28].

1.4.3 Cell labeling

External labeling of cells with quantum dots has proven to be relatively simple, but intracellular delivery adds a level of difficulty. Several methods have been used to deliver quantum dots to the cytoplasm for staining of intracellular structures, but so far these have not been particularly successful. Micro-injection techniques have been used to label xenopus [14] and zebrafish [29] embryos, producing pancytoplasmic labeling, but this is a very laborious task, which rules out high volume analysis. Quantum dots uptake into cell via both endocytic and non-endocytic pathways has also been demonstrated, but result in only endosomal localization.

In this thesis, we discuss several organic stabilizer for synthesizing CdTe quantum dots and their possible biological and photochemical applications, being used as the possible photosensitizer sensor for concentration determination and also lead sulfide (PbS) and possible applications as the CEA (cancer embryonic anitigen) sensor.

CHAPTER 2

CDTE SEMICONDUCTOR QUANTUM DOTS

2.1 Introduction

When considering biological applications, cadmium telluride (CdTe), this is a notorious name when it is caught on the first sight due to its toxicity, but only so if ingested, its dust inhaled, or it is handled inappropriately. If it is properly and securely encapsulated, CdTe may be rendered harmless. Nowadays, it became a very useful material in the thin film solar cell industry, or in infrared optical material for optical windows and lenses. Bulk CdTe is transparent in the infrared wavelength, from close to its bandgap energy which is approximately 1.44eV at 300K (i.e. 860 nm) to the wavelength greater than 20 μm, which is already in the infrared region. As it has been presented that if the size of the bulk CdTe material shrinks to nanometer scale, normally 2 to 5 nm, the bandgap energy of the material will increase, due to quantum confinement effect, meaning the fluorescence peak will shift towards the infrared region or even visible range. This will open a new gate of application for this magical semiconductor material to be used in several areas which require small things to penetrate. CdTe quantum dots are also highly luminescent nanoparticles with quantum yield up to 80% if the parameters through the synthesis process are carefully manipulated [30]. In this section, we are going to discuss about how this kind of quantum dots have been synthesized and its related biological applications based on the research which has been conducted through the years.

2.2 Reaction mechanism

The basics of the aqueous synthesis of thiol-capped CdTe quantum dots have been described in details in [7, 31, 32]. In a typical standard synthesis [32], $Cd(ClO_4)_2 \cdot 6H_2O$ (or any other soluble Cd salts) was dissolved in water in the range of concentrations of 0.02 M or less, and an appropriate amount of the thiol stabilizer was added under stirring, followed by adjusting the pH by dropwise addition of a 1 M solution of NaOH. The solution was placed in flask B fitted with a septum and valves and was deaerated by N_2 bubbling for 30 min. Then in flask A, solid bulk Al_2Te_3 reacted with diluted H_2SO_4 acid to generate H_2Te gas. See Fig 2.1. (Caution: since H_2Te is an extremely toxic gas, this experiment was conducted in a properly ventilated hood and proper protective approach such as lab suit, gloves, mask and goggles, etc

should be used.) First step, with the slow nitrogen flow, the H_2Te gas was gradually introduced into flask B to react the Cd-RSH precursor. The offgas of excess H_2Te was collected by NaOH solution to avoid being let out to ambient environment. Second step, after approximately 10 min later when there was no more H_2Te gas generated in flask A, the tubes were dissasembled and flask B was connected with the water cooling condenser and the CdTe quantum dots precursor solution were heated to promote crystal growth. See Fig 2.1.

The chemical reactions undertaken in this experiment are as follows.

$$Cd^{2+}+H_2Te \xrightarrow{HS\text{-}R} Cd\text{-}(SR)_xTe_y+2H^+ \quad (2.1)$$

$$Cd^{2+}+NaHTe \xrightarrow{HS\text{-}R} Cd\text{-}(SR)_xTe_y+H^++Na^+ \quad (2.2)$$

$$Cd\text{-}(SR)_xTe_y \xrightarrow{100^\circ C} \text{CdTe quantum dots} \quad (2.3)$$

$$Al_2Te_3+H_2SO_4 \longrightarrow Al_2(SO_4)_3+3H_2Te\uparrow \quad (2.4)$$

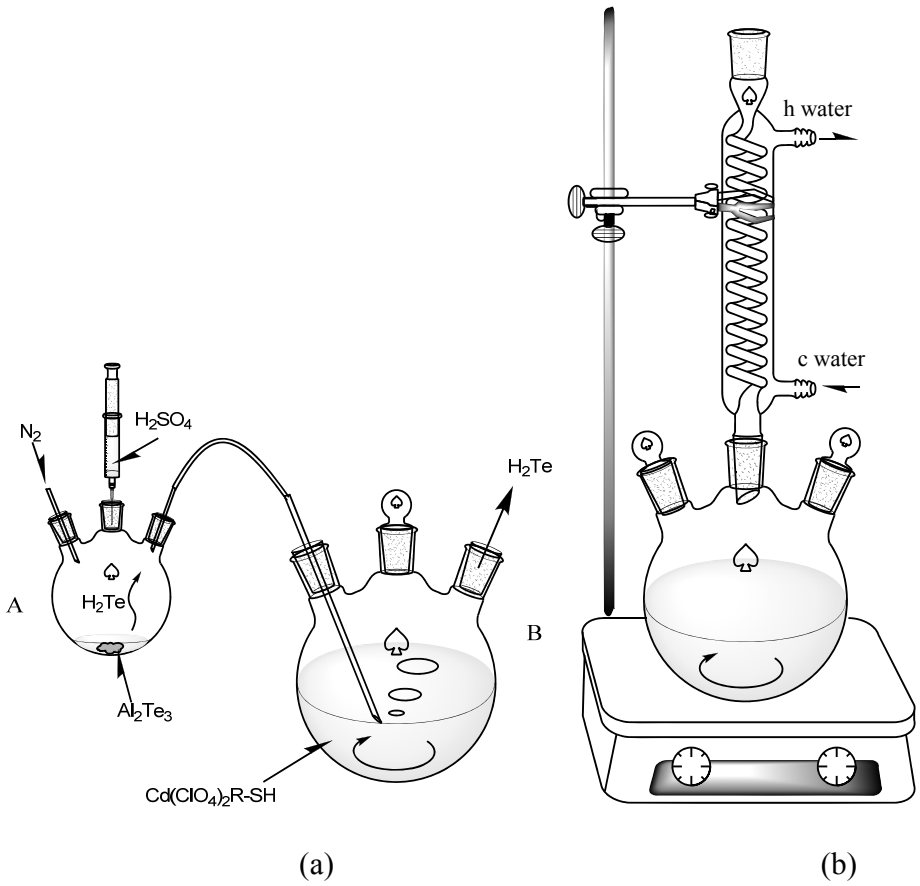

Fig 2.1 Schematic presentations of thio-capped CdTe quantum dots.
(a) 1st step: formation of CdTe precursors by introducing H_2Te gas into the aqueous solution of Cd precursors complexed by thiols. (b) 2nd step: heating and stirring to achieve quantum dots growth and crystallization. [32]

The important part of this setup was the connecting tube for introducing the H_2Te gas, which should be as short as possible and the tube should be made of glass or another inert material. The use of glass joints and connections is strongly recommended due to the high reactivity of H_2Te gas with rubber and common polymer tubes. The use of relatively small and well-deaerated flask for the generation of H_2Te may also help to reduce undesirable losses of this gas. Special precautions should be taken against the possible leakage of the non-reacted H_2Te. We note that the synthetic procedure described above is easily up-scalable. Meanwhile, H_2Te gas can be generated for the synthesis of CdTe quantum dots as well as other tellurides, like HgTe [33, 34] or ZnTe [35] taking advantage of reaction (2.4).

2.3 Experimental Section

CdTe quantum dots could survive in many different environments, depending on what ligand they attach to. In order to be better suited for biological applications, only aqueous soluble CdTe quantum

dots have been synthesized. But with different ligands we have the option to allow the quantum dots to be stabilized in many different pH values. The most frequently used organic thiol capping ligands are thioglycolic acid (TGA), mecaptoacetic acid (MPA), L-Cysteine or 2-mercaptoethylamine (or cysteamine, namely CA). Both TGA and MPA allow the synthesis of the most stable (typically, for years) aqueous solutions of CdTe quantum dots possessing negative charge due to the presence of surface carboxylic groups. Cysteamine-stabilized quantum dots possess moderate photostability (although they may be stable for years as well being kept in darkness) and attract an interest due to surface amino-functionality and positive surface charge in neutral and slightly acidic media. Other thiol stabilizers are mainly used when some specific functionalities are envisaged, the over view of them may be found in [32].

2.3.1 Synthesis of water soluble CdTe quantum dots

Cadmium perchlorate hydrate ($Cd(ClO_4)_2 \cdot 6H_2O$), thioglycolic acid (TGA), sodium hydroxide (NaOH), L-Cysteine, mercury perchlorate hydrate ($Hg(ClO_4)_2 \cdot H_2O$) were purchased from Sigma-Aldrich, St. Louis, MO, USA. Al_2Te_3 lump material and 2-Mercaptoethylamine hydrochloride (CA) were purchased from Alfa Aesar, Ward Hill, MA. H_2SO_4 (95~98%) was purchased from Pharmo-APPER Company. All chemicals were used as received without any further purification process. Please refer the chemical structure of the three kinds of stabilizers as in Fig 2.2.

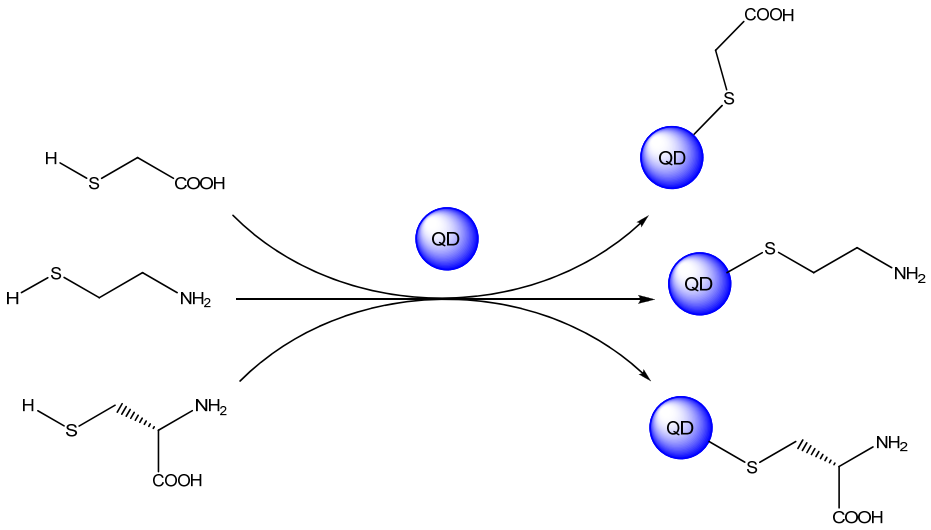

Fig 2.2 Schematic representation of the CdTe quantum dots with three kinds of stabilizers

2.3.1.1 TGA stabilized CdTe quantum dots

The setup used was described in Section 2.2. Dissolve 4.70 mmol (1.973 g) of $Cd(ClO_4)_2 \cdot 6H_2O$ into 250 mL deionized water in a beaker. After the Cd precursor salt had been fully dissolved to result a clear solution, 793.9 μL of thioglycolic acid (TGA) (11.4 mmol) with concentration of 98% was added, and solution become turbid with white color. The pH value of the solution was carefully adjusted by adding of NaOH solution dropwisely with concentration of 0.5 M until it reached 11.5. Then the solution was transferred into a 500 mL three neck flask. The solution was bubbled with nitrogen or Ar inert gas for approximately 30 min. The H_2Te gas was introduced with the inert gas flow from flask A into flask B by adding 3 mL of 0.5 M H_2SO_4 into flask A which had 0.4 g Al_2Te_3 power in it using a injector puncturing through the plastic stopper. Then the solution became red-orange instantaneously in flask B. Continue introducing the gas for 5 to 10 min until there was no more H_2Te generated. Then tubes were disassembled on flask A and flask B. While continue stirring, a condenser and two stoppers were attached on flask B and heating was started in order to raise the temperature of the solution to 100 ℃ for different period amount of time for the quantum dots to initiate the particle growth. The solution gave off green luminescence after exposing by UV light bulb after heating for 30 min and red luminescence after heating for 30 hours. After that, continuous heating decreased the luminescence intensity.

2.3.1.2 L-Cysteine stabilized CdTe quantum dots

The process is similar as the one described previously in Section 2.3.1.1 as using the TGA as the stabilizer, but with only a modification of replacing TGA with L-Cysteine of 1.379 g (as 11.4 mmol). Note: L-Cysteine is a special amino acid and need to be stored in the fridge with the temperature to be around 4 ℃. Storing in ambient temperature will result deterioration of this chemical and the solution will become turbid even the pH value has been adjusted to 11.5.)

Compared with ones stabilized by TGA, L-Cysteine stabilized CdTe quantum dots grow much faster. It takes approximately 7 hours for the quantum dots to reach the same red color as the ones stabilized by TGA.

2.3.1.3 CA stabilized CdTe quantum dots

The recipe for synthesizing the CA stabilized CdTe quantum dots is similar to that of the TGA stabilized ones. There are two modifications. One is to use 1.295 g (11.4 mmol) CA instead of TGA. The other is to modify the pH value to be 6.00 for adjusting the Cd precursor before introducing H_2Te gas.

The chemical affinity of CA on the CdTe quantum dots is not as good as TGA. Therefore, after the H_2Te gas introduction, small lumps of quantum dots agglomeration appeared. In that case, just right before the heating process, the coarse quantum dots solution was centrifuged with 3000 rpm to get rid of the agglomeration. The clear, transparent orange like supernatant solution was transferred back into flask B for heating. As heating goes on, the color of the solution became darker into red, and the luminescence it gave off tuned from green to red when exposed by UV light bulb.

2.3.2 Synthesis of water soluble CdHgTe quantum dots

By using the quantum dots synthesized previously, we could obtain CdHgTe infrared emission quantum dots by the following method. First dissolve $Hg(ClO_4)_2 \cdot H_2O$ into deionized water to make 25 mM solution. Then add the Hg precursor solution into the CdTe quantum dots solution with three kinds of stabilizers: TGA, L-Cysteine and CA respectively. Note: adding Hg will result luminescence intensity drop so, it is better to add small amount first (e.g. 20 μL) and then stir the sample for 10 min and then add another time. Monitor the emission peak for the whole process until the emission peak red shifts to the final desirable wavelength.

2.4 Characterization Section

Photoluminescence spectra were obtained from Shimadzu RF-5301PC Spectrofluorophotometer with 400W monochromatized xenon lamp. UV absorption spectra were measured by UV-2450 Spectrophotometer E120V, Shimadzu. UV Quartz cuvettes, with 1 mm path length, inside width 10 mm and 45×12.5×12.5 mm dimension, were used for both optical properties measurement. Transmission electron microscope (TEM) images were taken by JEOL JEM02100 instrument, with an accelerating voltage of 200 kV. Samples for TEM were prepared by depositing a drop of CdTe quantum dots solution onto a carbon-coated copper grid. The excess liquid was wiped away with filter paper and the grid was dried in air.

2.5 Data Analysis and Discussion

2.5.1 Transmission electron microscopy

Heating process will promote CdTe quantum dots particle growth, as well as crystallize the particles, as it could be seen clearly in Fig 2.3. With different heating time, 65 min, 6.5 h, 14 h, 23 h respectively, the quantum dots size grew from the approximately 2 nm core to approximately 6 nm in the end for the 23 h sample.

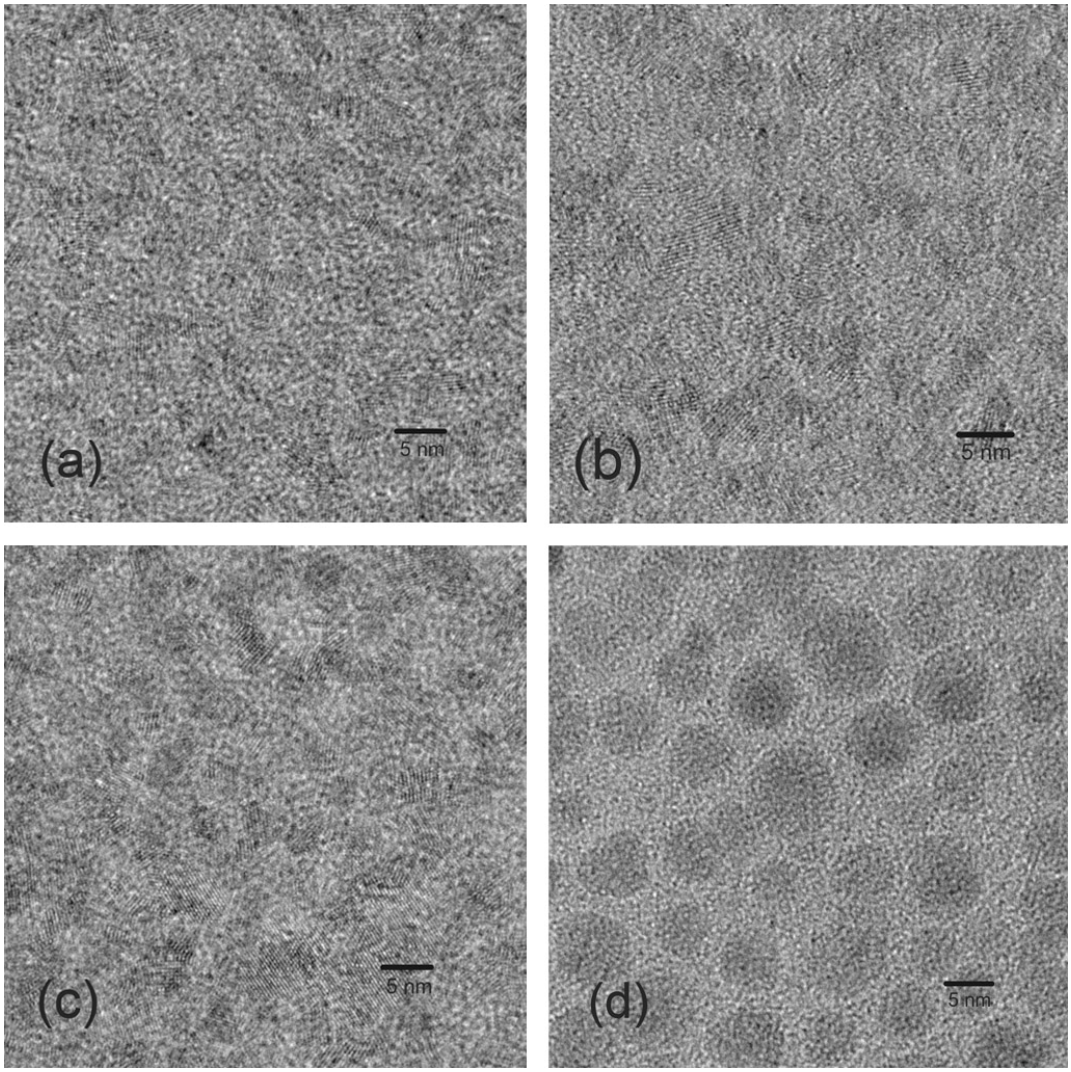

Fig 2.3 TEM overview of the TGA stabilized CdTe quantum dots with different reaction time (a) 65 min, (b) 6.5 h, (c) 14 h, (d) 23 h. Bar width 5 nm respectively.

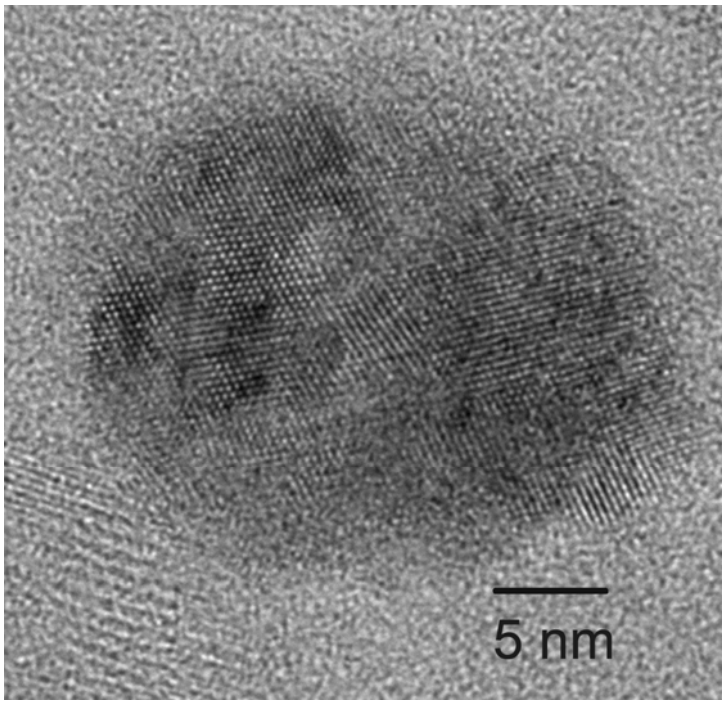

Fig 2.4 TEM image of the CdTe/T 0711 quantum dots

High resolution transmission electron microscope (HRTEM) image was taken for the TGA stabilized quantum dots, and the stack layers of the zinc blend structured CdTe atoms could be seen from Fig 2.4, with low crystal defects. Fig 2.5 shows the energy dispersive X-ray (EDX) analysis of the CdTe quantum dots, bearing the ingredient of the particle to be completely composed of Cd and Te element.

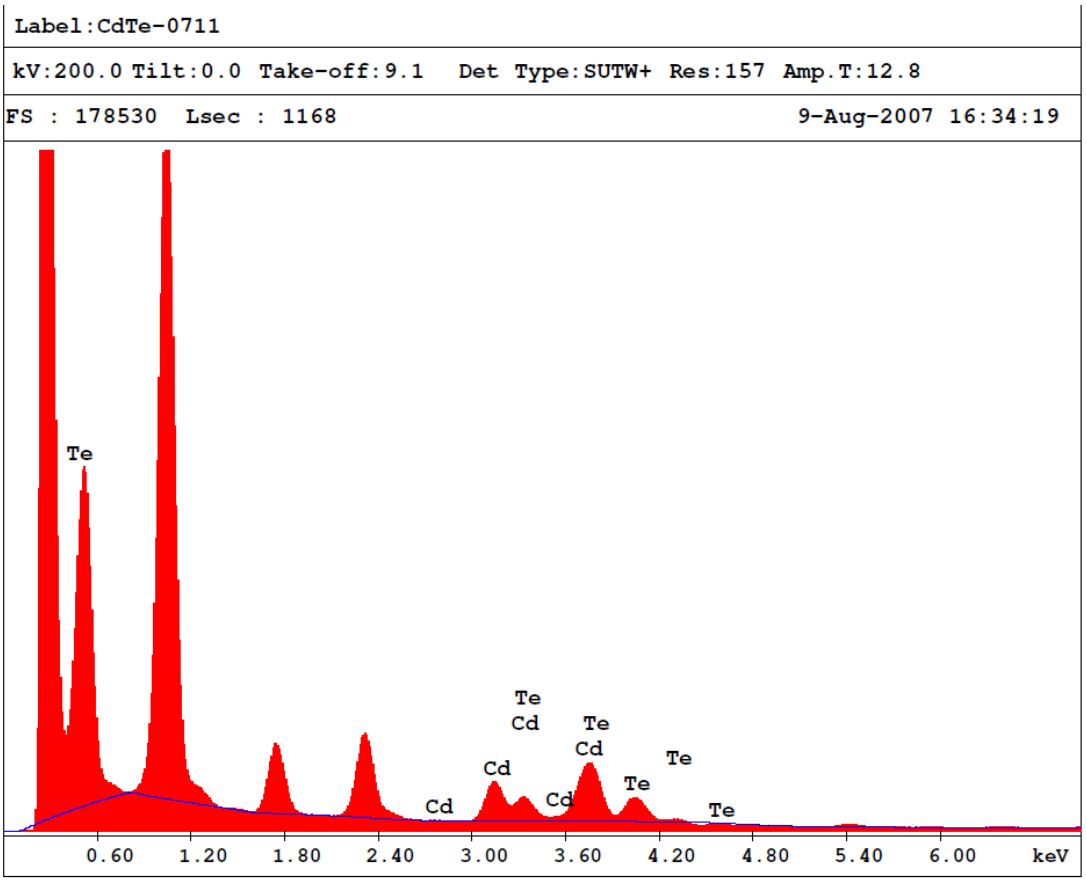

EDAX ZAF Quantification (Standardless)
Element Normalized
SEC Table : Default

Element	Wt %	At %	K-Ratio	Z	A	F
CdL	30.13	32.87	0.2665	1.0267	0.8271	1.0416
TeL	69.87	67.13	0.3894	0.9882	0.5641	1.0000
Total	100.00	100.00				

Element	Net Inte.	Bkgd Inte.	Inte. Error	P/B
CdL	97.80	31.86	0.38	3.07
TeL	157.90	32.79	0.28	4.81

Fig 2.5 EDX analysis quantification of the CdTe quantum dot

2.5.2 Photoluminescence spectra

Emission photoluminescence spectra for all four samples are shown in Fig 2.6 by using excitation wavelength of 460 nm, excitation slit 1.5 nm as well as emission slit 1.5 nm, emission photoluminescence spectra for all four samples could be obtained as shown in Fig 2.6.

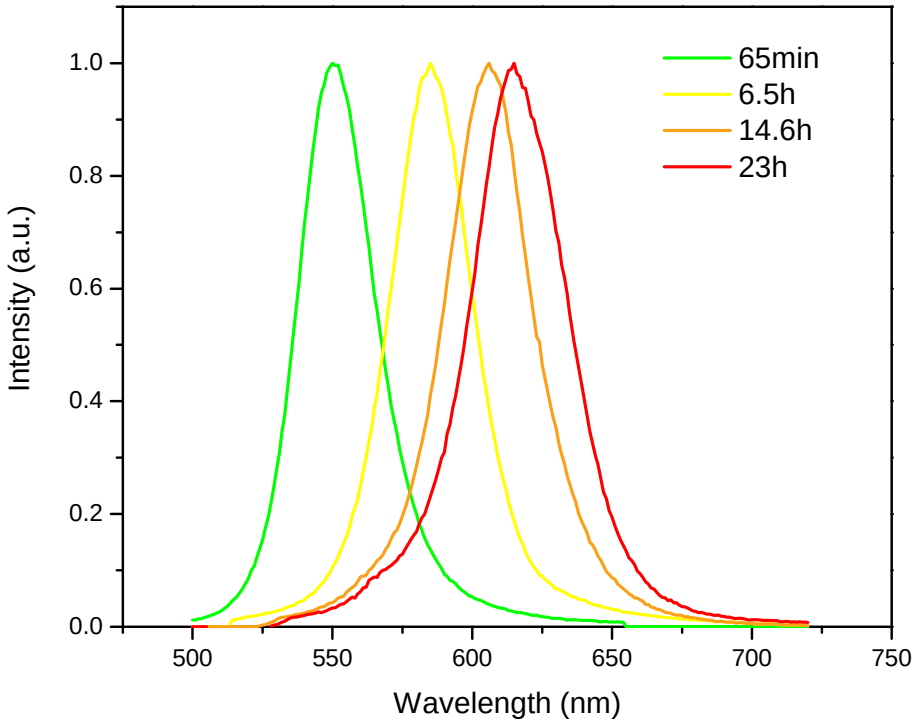

Fig 2.6 Photoluminescence emission spectra for TGA stabilized CdTe quantum dots solution

As we discussed earlier, the heating procedure promotes quantum dot size to grow larger and therefore decreases the bandgap energy and shifts the emission wavelength from green to red, or even infrared. Fig 2.6 shows the photoluminescence spectra for TGA stabilized CdTe quantum dots. For the same sample, while maintaining the reaction temperature to be 100℃, four samples were collected for different amount of heating time period, 65 min, 6.5 h, 14.6 h, 23 h respectively.

Table 2.1 Peak wavelength and FWHM for four CdTe quantum dots

	65 min	*6.5 h*	*14.6 h*	*23 h*
Peak wavelength	550 nm	585 nm	606 nm	615 nm
FWHM	30 nm	34 nm	35 nm	39 nm
FWHM range	536 ~ 566 nm	568 ~ 602 nm	588 ~ 623 nm	597 ~ 636 nm

Table 2.1 indicated that, the full width at half maximum (FWHM) values for the four samples are actually increasing with longer heating time. The 65 min sample shows 30 nm FWHM which is almost as good as 5% of quantum dots size distribution. As the heating time goes by, more and more particles are prone to grow with different rate, resulting broad size distributions. When the heating time reached 23 h, inhomogeneous broadening has increase the FWHM to as much as 39 nm.

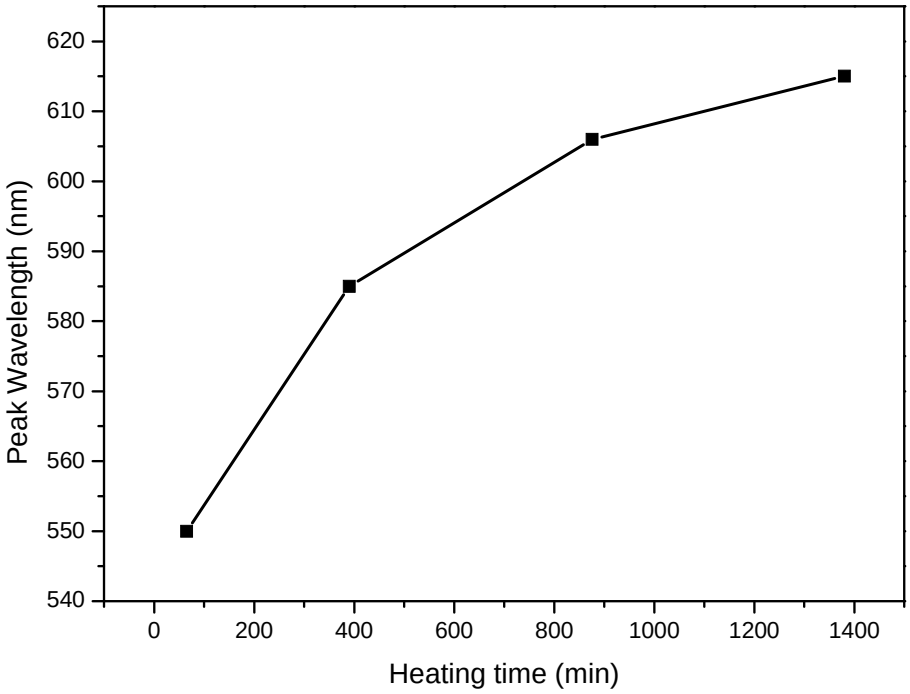

Fig 2.7 Peak wavelength versus Heating Time for TGA stabilized CdTe quantum dots

2.5.3 Red shift phenomena of Hg^{2+} adding approach

As quantum dots grow larger, their emission peaks red shift. But from Fig 2.7 we could see that by given longer time, the rate which the emission peak shifts decreases. After almost one day, the quantum dots nearly stopped growing as illustrated 23 h (1400 min) when the curve has almost reached a plateau. Infrared emission quantum dots are very useful [36, 37], but even though the emission peak of the quantum dots could be easily tuned by simply enlarge their sizes, this is not always an effective approach. Promoting particle growth further after 23 h, not only the FWHM increases, resulting broadening of the particle size distribution, but also the emission intensity drops dramatically (not shown in the figure). Therefore, in order to make near infrared (NIR) emission quantum dots, we need to seek

for more methods. One of them is to dope mercury within the quantum dots to further decrease the bandgap energy, as we have been discussed in Section 2.3.2.

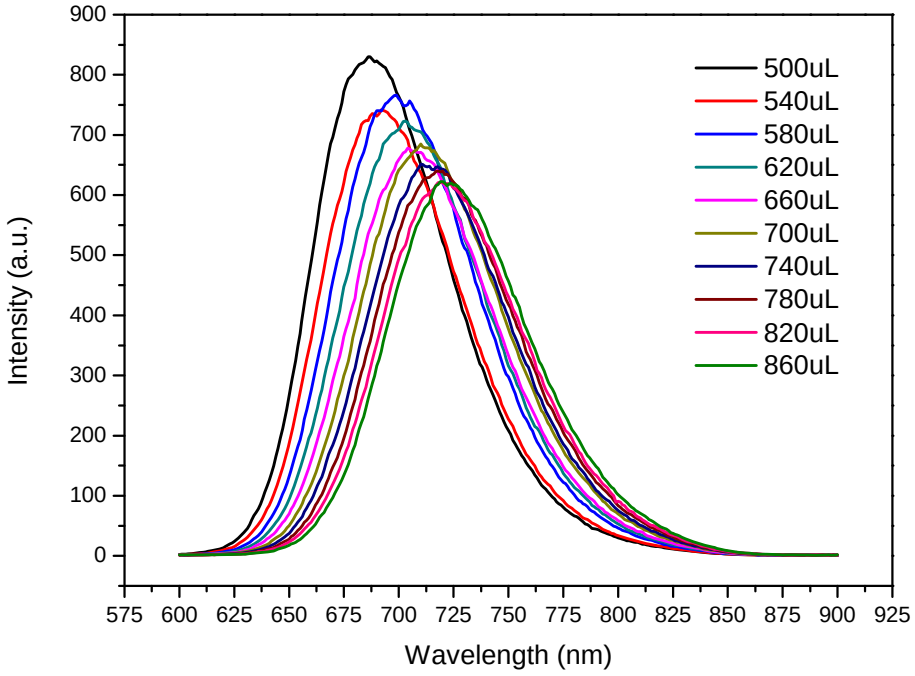

Fig 2.8 Photoluminescence emission spectra for CdTe quantum dots stabilized by CA, when different amount of $Hg(ClO_4)_2$ 25 mM solution was added, excitation wavelength 575 nm

When different amount of $Hg(ClO_4)_2$ 25 mM solution was added to the CdTe quantum dots solution with CA as the stabilizer, the emission peak keeps red shifting until the free Hg^{2+} ion concentration has become saturated within the quantum dots solution. Susha [38] et al has done some research about using the CdTe quantum dots as a possible ion detector and because the solubility product constant K_{sp} for HgTe, is much slower (approximately 20 times) than the one for CdTe, the free Hg^{2+} ions in the solution slowly replaced the Cd^{2+} ions on the CdTe quantum dots surface; consequently we have $Cd_xHg_{1-x}Te$ alloyed quantum dots with x% of Cd in their ingredient.

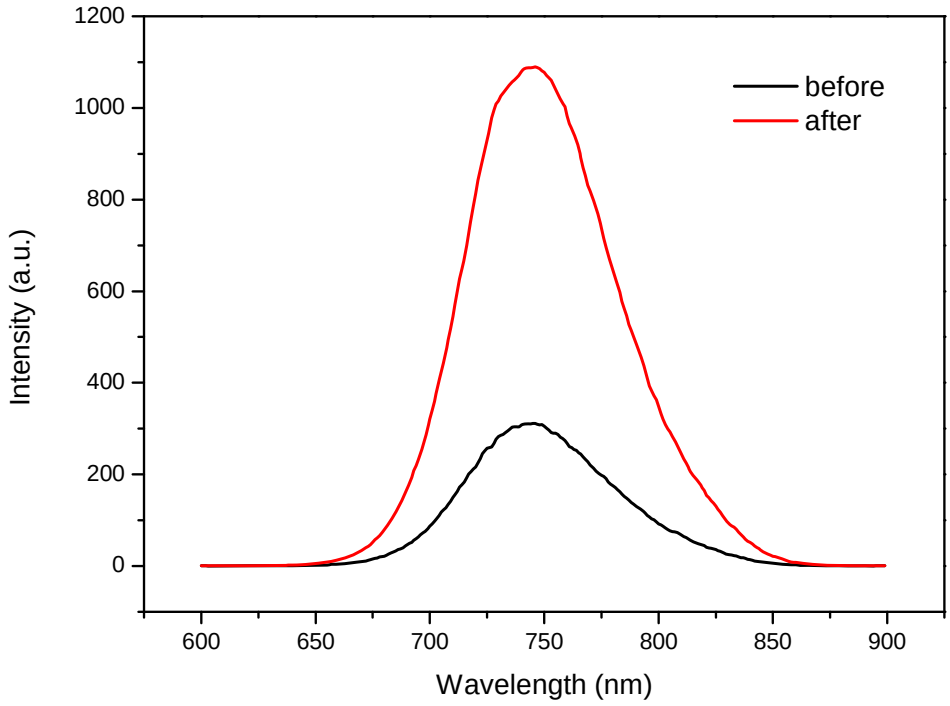

Fig 2.9 Photoluminescence emission spectra for $Cd_xHg_{1-x}Te$ quantum dots comparison, with excitation wavelength 575 nm, "after" relates to the spectrum 4 days later

Storing the $Cd_xHg_{1-x}Te$ solution for 4 days in the fridge after being injected 860 μL Hg^{2+} solution, the luminescence intensity almost increased 3.5 fold while the emission peak almost remains unchanged, as seen from Fig 2.9 (Black curve corresponds to the PL spectrum for the freshly prepared sample, and the red curve corresponds to the PL spectrum for the sample which has been stored in the fridge for 4 days.) This indicated that more time allowed for further replacement of the Cd^{2+} ions with Hg^{2+} ions, less interactions will be influenced by the quantum dots themselves with the dissociated Hg^{2+} ions.

By introducing this type of simple approach, we could carry on the tuning process to shift the emission wavelength to near infrared region, without decreasing the luminescence intensity as much as the heating process. To further understand this process, we carry on an experiment as follows.

Instead of adding 140 μL Hg^{2+} solution (with concentration 25 μM) into 3mL CdTe quantum dots solution (stabilized with CA) at one time, we separately add 10 μL each time for 14 times. And we measure the photoluminescence spectra after the solution has been stabilized for 1 min. The excitation

wavelength is 480 nm with excitation and emission slits to be 3 nm and 3 nm respectively. The spectra are collected are shown in Fig 2.10.

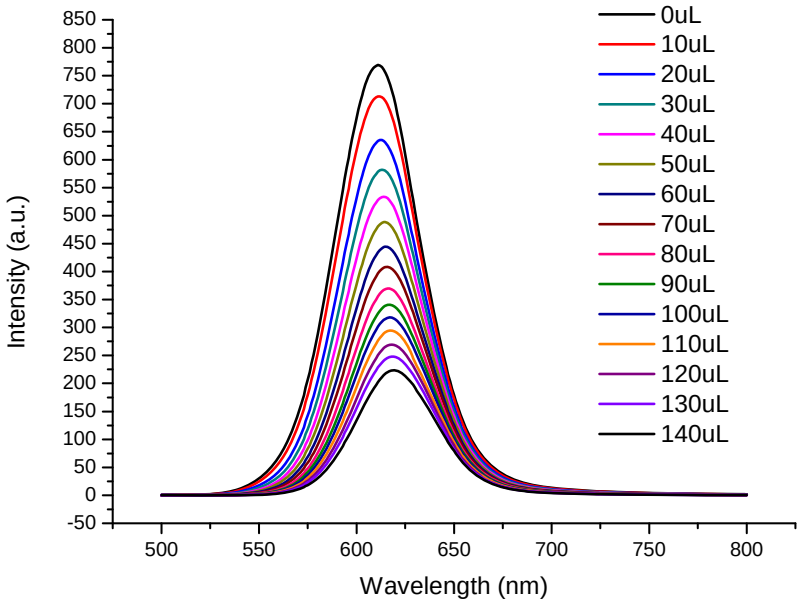

Fig 2.10 Emission spectra of CdTe/CA quantum dots when 10 μL Hg^{2+} was gradually added into the solution

As the volume of the Hg^{2+} added into the solution increases by 10 μL increment, the red shift of the emission peak is obvious. Using the wavelength to be the x-axis, the amount of the Hg^{2+} solution added to be the y-axis, and the photoluminescence emission intensity to be z-axis and construct a 3-D diagram of data is shown in Fig 2.11.

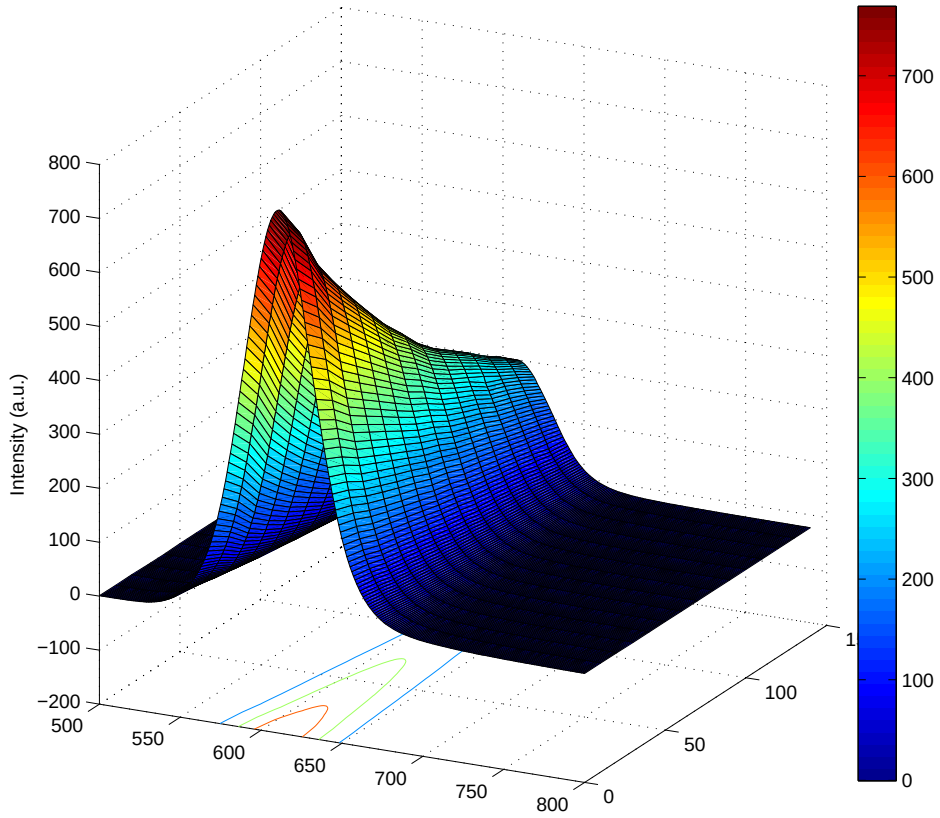

Fig 2.11 3-D plot of the photoluminescence intensity versus wavelength (x) and the Hg^{2+} volume (y)

The CdTe stabilized by CA quantum dots solution has been added 10 μL increment until the total amount of volume added reached 140 μL as Fig 2.11 shows. The intensity gradually decreases as the more and more Hg ions were added.

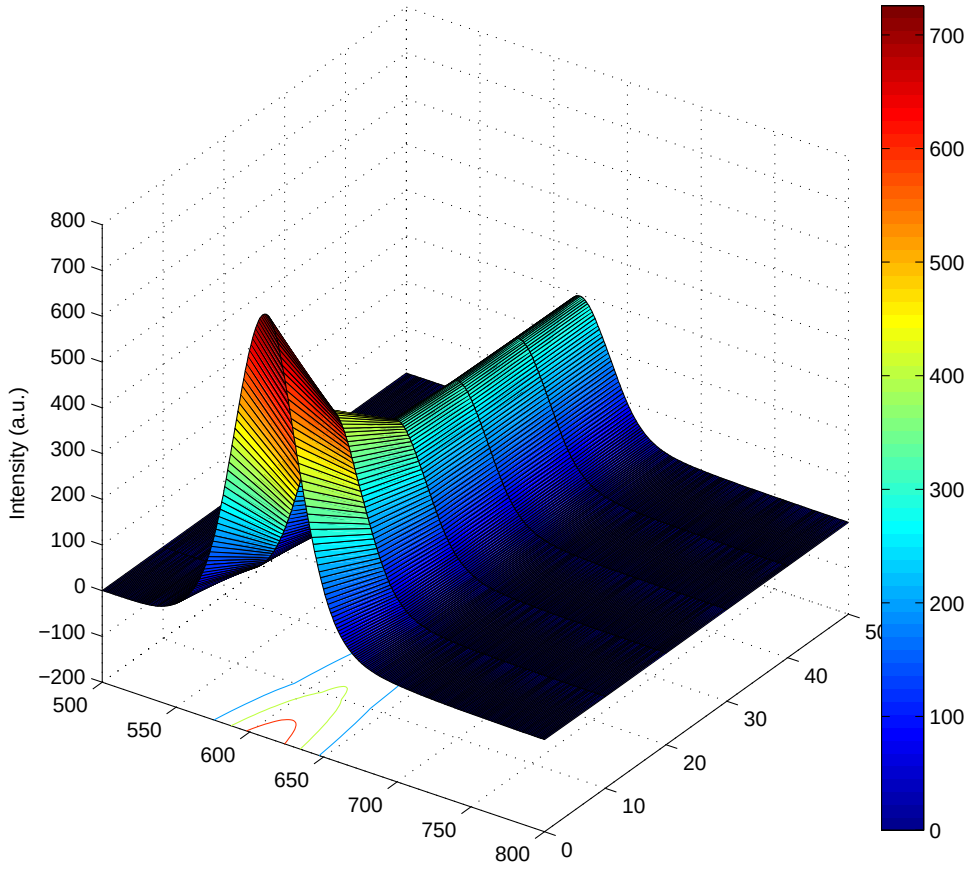

Fig 2.12 One time adding of Hg^{2+}, PL intensity versus wavelength (nm) and time (min)

Fig 2.12 shows the spectra for the sample which has been added 140 μL Hg^{2+} solution at one time. The x-axis is the wavelength, and the y-axis is the time after the reaction. It could be seen here that, at first the luminescence intensity drops dramatically, but after 10 or 20 min later, the intensity almost remains unchanged over time and the sample has reached a state of equilibrium.

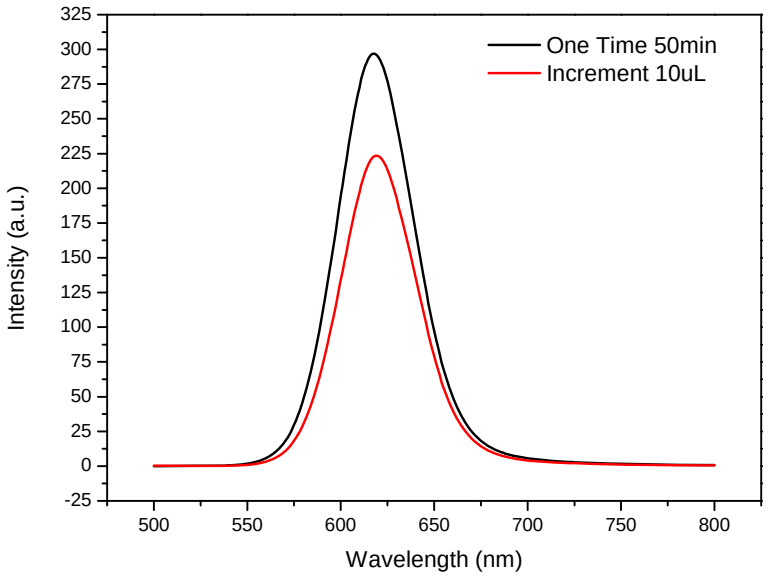

Fig 2.13 Final spectra compare, 140 μL Hg^{2+} solution added

After 140 μL Hg^{2+} solution was added for 50 min, the black spectrum has higher intensity than the red spectrum, which is the CdTe quantum dots solution added 14 times of 10 μL Hg^{2+} solution. This indicates that, more surface defects will be generated if we divided one amount of Hg^{2+} solution into several small amounts, as shown in Fig 2.13.

This is because the dissociated Hg^{2+} ions will slowly replace the Cd on the quantum dots surface, with different lattice constant on HgTe and CdTe, the replacing process will certainly create defects and crystal lattice dislocation on the quantum dots surface.

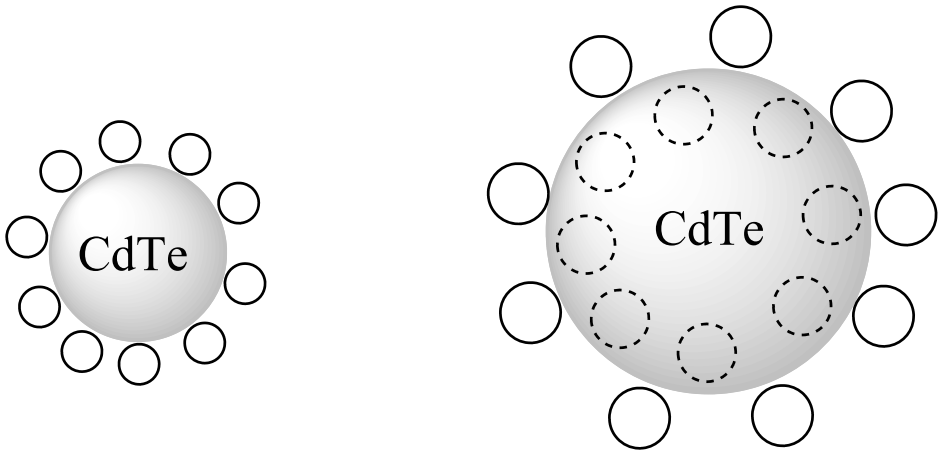

Fig 2.14 Schematic diagram of the Hg^{2+} ions replacement mechanism (First setting: one time, second setting: multiple times)

When the Hg^{2+} ions were added at one time, it could be illustrated by the first setting from Fig 2.14. The CdTe quantum dots have been coated by one solid HgTe shell, impeding the Hg ions from penetrating into the inner core of the CdTe quantum dots, which maintains higher luminescence intensity. If we use the "multiple times" strategy, the much thinner layer of HgTe shell has not been fully formed and then another thinner layer of HgTe shell has added on it, making it has more surface defects and dislocations on the crystal lattice matching between CdTe and HgTe. Even though it is not obvious seen here we can expect that, since the scheme of "multiple times" has slightly lower luminescence intensity than "one time" scheme, it should be more red shifted than the former because of its gradient Hg concentration within the outer shell of the CdTe quantum dots. This could suit for different requirements. We have to optimize the parameters of how much Hg^{2+} ions should be added and how many small amounts we need to split into, in order to get high quantum yield near infrared emission quantum dots. So far the near infrared emission CdTe quantum dots which is the most luminescent is the one stabilized by CA, with Hg^{2+} adding protocol slightly modified and optimized. Its spectrum is given in Fig 2.15 with excitation wavelength at 580 nm.

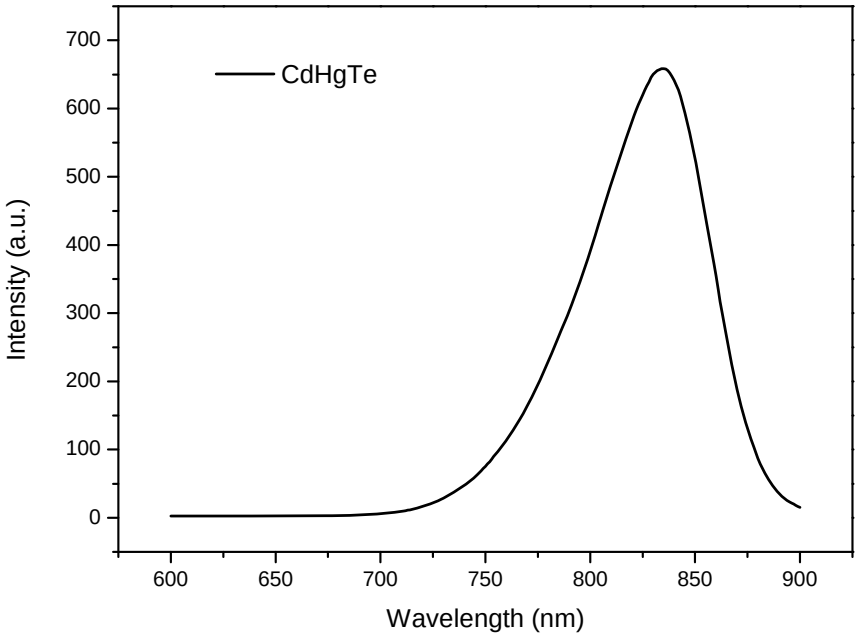

Fig. 2.15 Optimized scheme of the synthesizing the high quality near infrared emission quantum dots The emission wavelength could be tuned to reach 834 nm if the parameters are optimized.

2.6 Conclusion

CdTe quantum dots with different stabilizers such as thioglycolic acid (TGA), L-Cysteine and 2-mercaptoethylamine (CA) have been synthesized. Because they are stable at different pH ranges (TGA pH=11.5, L-Cysteine pH=11.5, CA pH=6.0), they can suit for different applications. For example, in most biological systems the most frequently encountered pH value is 7. Therefore the CA stabilized quantum dots are better suited for biological applications such as in vitro imaging and in vivo sensor. Mercury doped CdTe quantum dots, namely alloyed $Hg_xCd_{1-x}Te$ quantum dots have also been synthesized. Two methods of conducting the doping approach have discussed and it was discovered that by splitting the amount of Hg^{2+} ions solution into small amounts, red shift will be more obvious while luminescence intensity will slightly decrease.

CHAPTER 3

PDT RELATED APPLICATION OF CDTE QUANTUM DOTS

In this chapter, we review one of the innovative approaches for treating cancer: photodynamic therapy (PDT), and introduce quantum dots as a possible photosensitizer sensor. Since quantum dots intrinsic property of giving off luminescent signal which is subjected to the bandgap energy and is irrelevant to the excitation wavelength, quantum dots serve as possible biological assays or molecular sensors, as we have seen from the previous chapter. In this chapter, we investigate the possible biological application of the quantum dots as a photosensitizer assay.

3.1 Photodynamic Therapy for Cancer

Photodynamic therapy (PDT), as the name implies, is the treatment of cancer by using appropriate wavelength of light. It is a non-invasive approach of treatment that is less harmful to the body than other types of cancer treatments, such as radiotherapy and chemotherapy. The procedure includes two steps. Step one involves injecting a photosensitive drug (called photosensitizer) to the patient, which sensitizes cells to the effects of light. Step two involves subjecting the patient injected with the photosensitive drug to the laser light, which is then focused on the tumor and kills the cancer cells. The technology has advanced in recent years with the introduction of small fiber-optic cables that direct the laser beam to tumors in more remote areas of the body.

Here is where photosensitizers come into play. Because light is a form of energy: molecules of certain photosensitizers have the ability to absorb a photon of visible light energy and then transfer most of their absorbed energy to a molecule of oxygen, and transform it into a relatively strong oxidizing agent known as singlet oxygen, $^1O_2$. PDT takes advantage of the singlet oxygen and makes it kill the cells which forget to die—cancer cells. The excited states of both the photosensitizer and singlet oxygen have very short life time. In order to be effective enough, molecules of both species must be in very close proximity to the tumor cells. Moreover, the primary damage to cells occurs only while they are actually being exposed to the photoactivating light, although this effect may continue long after the treatment light has been turned off.

3.2 Experimental Section

3.2.1 Materials section

Protoporphyrin-IX (PPIX), tetraethyl orthosilicate (TEOS), ammonium hydroxide ($NH_3 \cdot H_2O$) was purchased from Sigma-Aldrich, Singlet oxygen sensor green (SOSG) was purchased from Invitrogen Corp, CA, USA. Sodium azide (NaN_3) was also purchased from Sigma-Aldrich, Fluka brand.

3.2.2 Silica coated quantum dots

In this experiment, the recipe of coating the TGA stabilized CdTe quantum dots with silica shell was modified from Yang et al [39]. Briefly, TGA stabilized CdTe quantum dots synthesized as described in Chapter 2 were used. Then add 500 μL of $NH_3 \cdot H_2O$ and 200 μL of TEOS were added to 20 mL TGA stabilized CdTe quantum dots solution. After this process, a thin layer of silica will be coated on the quantum dot surface.

3.2.3 Singlet Oxygen Sensor Green solution preparation

SOSG solution (~5 mM) was prepared using one vial out of the packaging box from the -20 ℃ freezer and add 33 μL of methanol. Addition of 792 μL of deionized water to further diluted the solution to 200 μM to make a stock solution. 20 μL of SOSG stock solution has been added to 3 mL of solution to be investigated, so the final concentration of the SOSG within the detection medium was approximately (20/3000)×200 μM=1.33 μM, which is within the range of the starting concentration (1~10 μM) from the instruction manual [40].

3.3 Results and Discussion

3.3.1 CdTe quantum dots response to protoporphyrin-IX

We have synthesized three types of quantum dots, with three kinds of stabilizers (TGA, L-Cysteine, CA, respectively). By monitoring their response to the protoporphyrin-IX, we found the working curve of the quantum dots luminescence intensity to the concentration of the protoporphyrin-IX content.

Concentrations from 0.05 mM to 0.35 mM with increment of 0.05 mM PPIX standard solution have been prepared. For the same amount of 3 mL CdTe quantum dots stabilized by TGA solution, 80 μL of PPIX standard solution was added into the quantum dots solution, then monitor the luminescence intensity spectra.

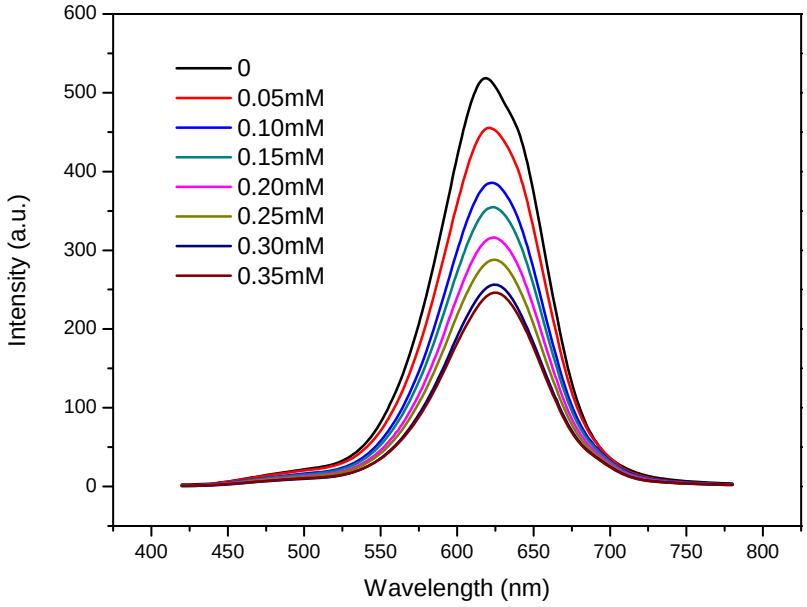

Fig 3.1 Luminescence response of CdTe/TGA due to PPIX with different concentration

Using the 400 nm as the excitation wavelength, luminescence spectra for various concentrations of PPIX solution added into quantum dots solution were obtained and are presented in Fig 3.1. After that, at each specific concentration the peak intensity has been recorded because it is the intrinsic property the quantum dots described.

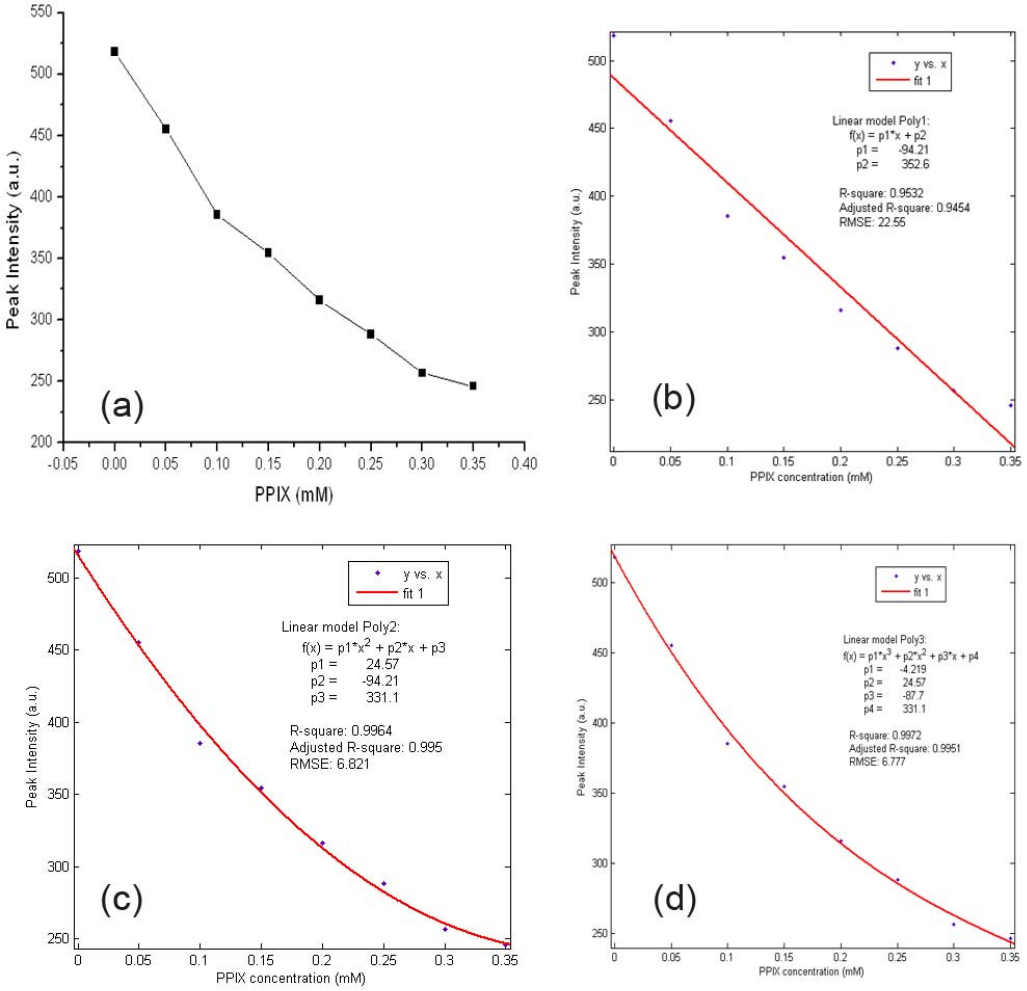

Fig 3.2 Different curve fitting approach for the peak intensity versus PPIX concentration
(a) No curve fitting (b) linear fitting (least square) (c) quadratic fitting (d) cubic fitting

As shown in Fig 3.2 (a), the points are almost aligned to a straight line except for the last point, and Fig 3.2 (b) has already given the square of correlation constant 0.9532. While Fig 3.2 (c) and (d) are quadratic and cubic curve fitting approach, increasing the square of the correlation constant as high up to 0.9964 or higher. This is probably due to the saturation effect of the PPIX within the CdTe quantum dots solution. As the concentration goes higher, its ability of "killing" the luminescence weakens. Meanwhile, this also explains that, as the amount of PPIX added into the quantum dots solution is so little, just 80 μL compare to the volume of the solution which is 3 mL, the volume of the PPIX solution added will not affect the intensity as much as we expected as it will be seen later. For simplification, we use the linear

least square approach to fit the intensity maximum. The problem with that is its accuracy, shown by the correlation constant. For more accurate working curve fitting, quadratic or even cubic fitting should be used.

Adding PPIX 35 mM solution into three different kinds of quantum dots solution with increment of amount of 10 µL produced almost the same result, as shown in Fig 3.3, Fig 3.4, and Fig 3.5.

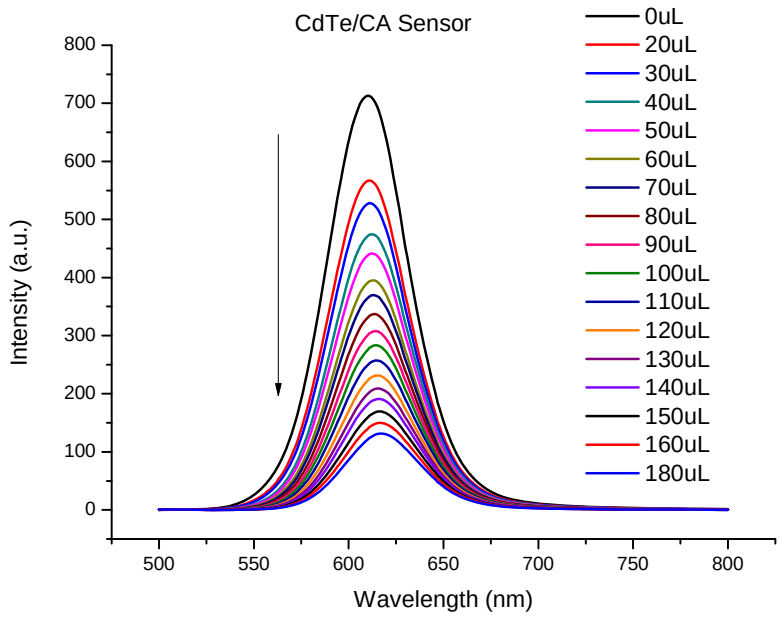

Fig 3.3 Luminescence response of CdTe/CA quantum dots with different amount of PPIX 35 mM solution (10 µL increment)

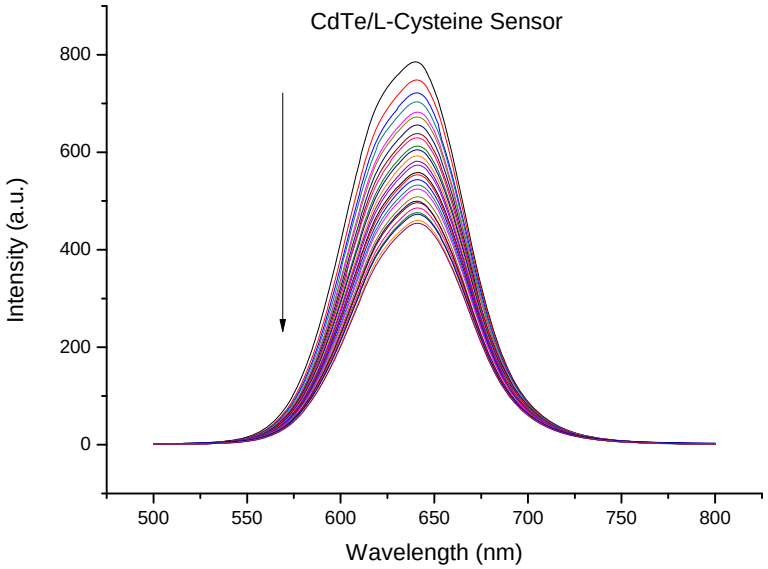

Fig 3.4 Luminescence response of CdTe/L-Cysteine quantum dots with different amount of PPIX 35 mM solution (10 µL increment)

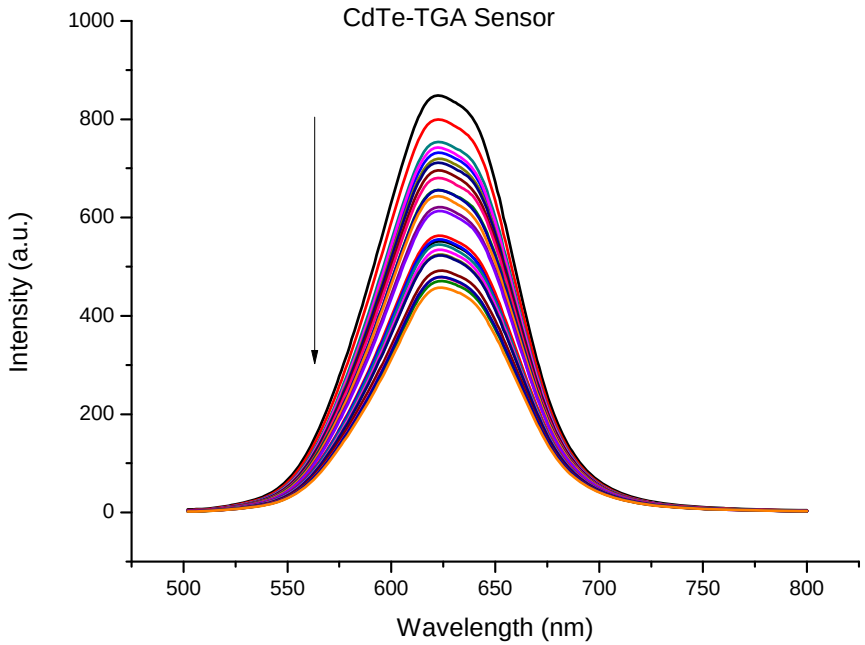

Fig 3.5 Luminescence response of CdTe/TGA quantum dots with different amount of PPIX 35 mM solution (10 µL increment)

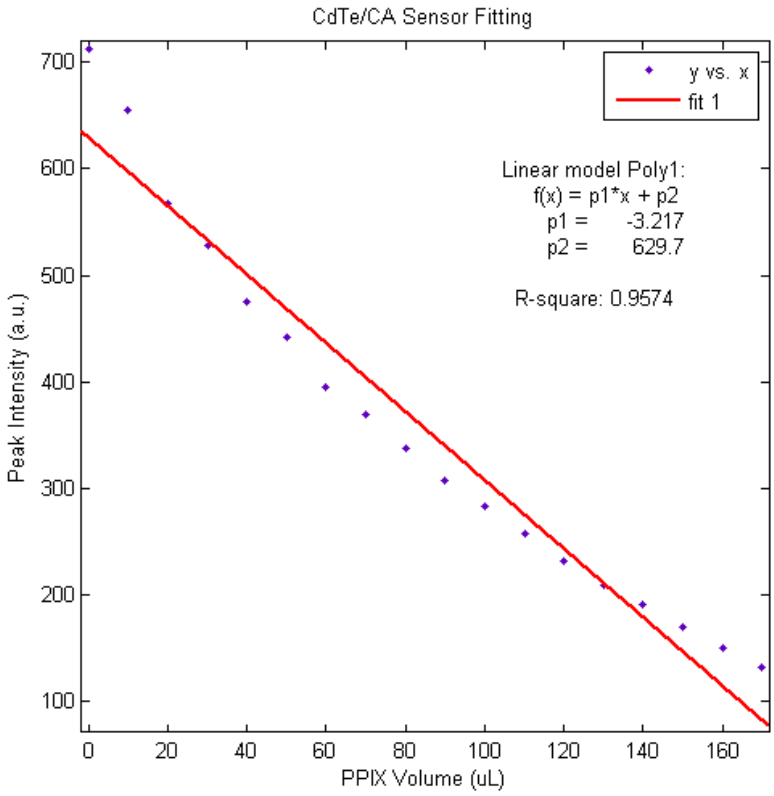

Fig 3.6 Least square fitting of CdTe/CA quantum dots peak intensity versus different amount of PPIX 35 mM solution (10 μL increment)

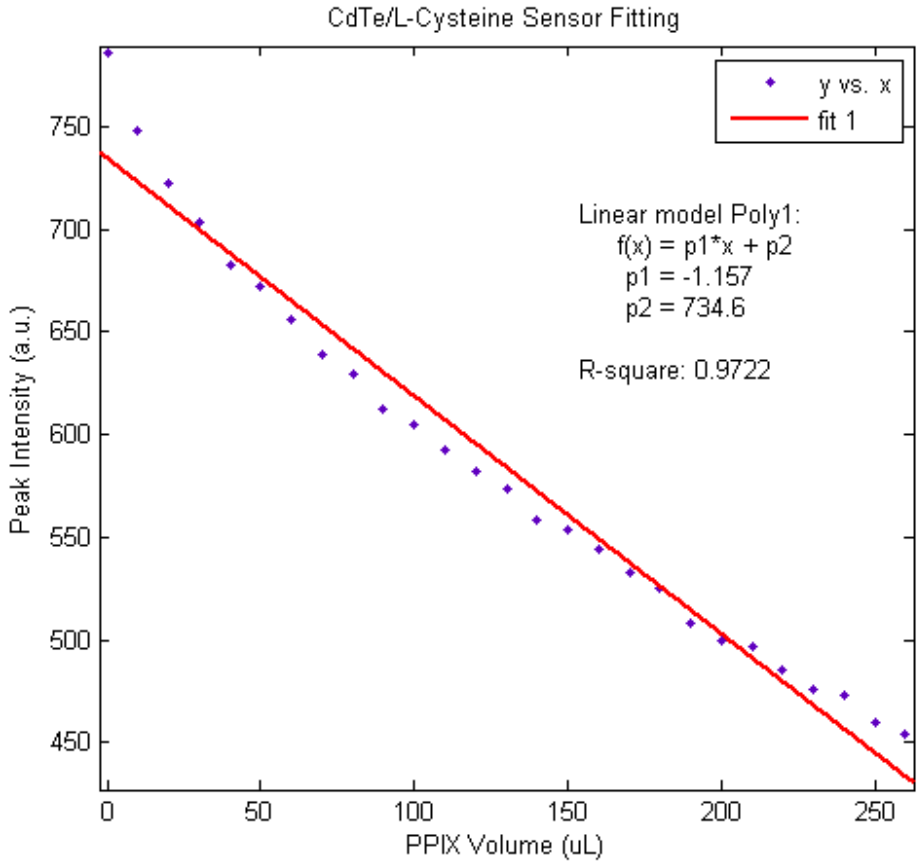

Fig 3.7 Least square fitting of CdTe/L-Cysteine quantum dots peak intensity versus different amount of PPIX 35 mM solution (10 µL increment)

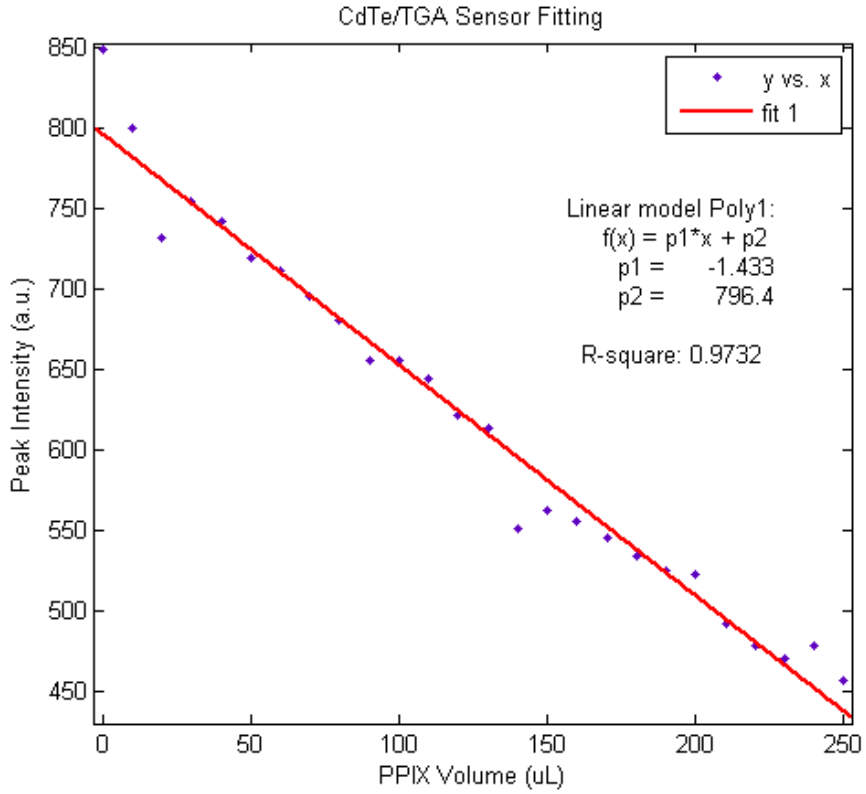

Fig 3.8 Least square fitting of CdTe/TGA quantum dots peak intensity versus different amount of PPIX 35 mM solution (10 μL increment)

After doing the least square fitting for the peak intensity with respect to the PPIX volume added in (shown from Fig 3.4, Fig 3.7 and Fig 3.8), the slope of the best fitted line is the indicator for the interaction between the PPIX and the quantum dots. Because these quantum dots are stabilized by different organic functional group, to some extent this indicator is related to the affinity of the organic stabilizer and the quantum dots. The biggest slope of all, which is -3.217 for the CdTe quantum dots stabilized by CA, explains why during the synthesis process there is possibility that agglomeration happens and centrifuge procedure is required to get rid of the large particles before the heating process. CA has relatively small affinity with the surface of the quantum dots compared with the TGA and L-Cysteine. The slopes for TGA and L-Cysteine are -1.433 and -1.157 respectively. It means that the quantum dots functionalized by these organic stabilizers are almost two times more stable than the one stabilized by CA. The correlation constant square, R square shows the linearity of the points considered. TGA and L-Cysteine stabilized quantum dots give higher R square values than the ones stabilized by CA.

At this time, we conclude that quantum dots which are more stable prone to be better sensors for assaying the concentration of the photosensitizers.

3.3.2 Silica coated CdTe quantum dots response to protoporphyrin-IX

In the experimental section we have synthesized silica coated CdTe quantum dots using the TGA stabilized quantum dots. The comparison of the luminescence response of this sample with the one without silica coating also offered important information about quantum dots stability and interaction with the photosensitizer .

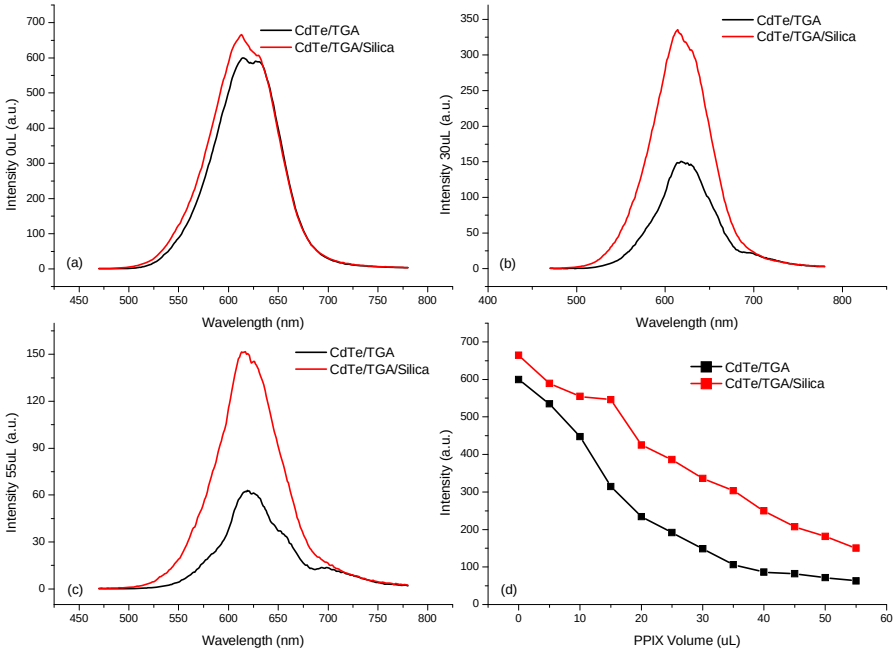

Fig 3.9 Comparison of the luminescence responses of the CdTe quantum dots with and without silica coating. (a), (b) and (c) are the spectra excited at 450 nm, added 0 µL, 30 µL and 55 µL of PPIX 35 mM respectively. (d) is the peak intensity with different amount of PPIX added.

As presented in Fig 3.9, at the beginning, the quantum dots with and without silica coating almost give the same intensity, the one with silica coating being slightly stronger than one without. After a certain amount of PPIX solution has been added, the intensity for both samples are starting to drop but no matter how much PPIX has been added, the one with silica coating always give stronger luminescence

than the one without silica coating, as shown in Fig 3.9 (b) and (c). Fig 3.9 (d) further strengthened this conclusion. This is probably because that silica coated quantum dots have less surface defects, meanwhile it provides protection layer for the inner core to be damaged by PPIX. Fig 3.10 further demonstrates that even with long period of radiation time, the CdTe quantum dots with silica coating showed no change in the luminescence intensity while the one without silica coating experienced photobleaching to some degree.

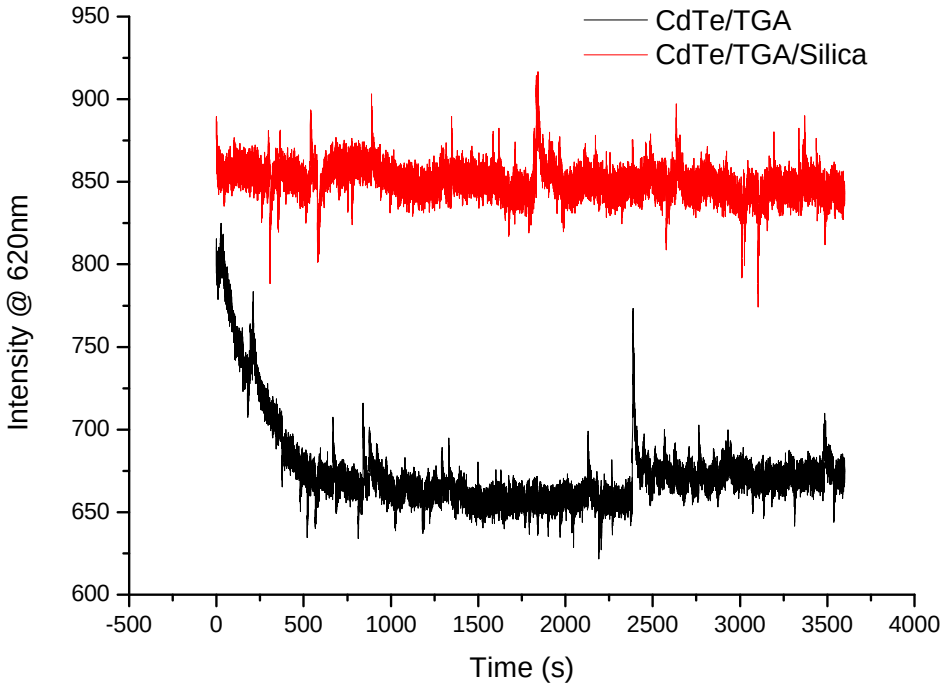

Fig 3.10 Excitation wavelength 620 nm, both samples are illuminated for 1 hr

3.3.3 Singlet oxygen detection using SOSG™, and CdTe quantum dots

We all know that PPIX is a widely used photosensitizer which can generate singlet oxygen. If we can prove that the loss of the luminescence intensity of the quantum dots is due to the amount of the singlet oxygen this photosensitizer generated, then quantum dots could be a better candidate for using as the potential singlet oxygen sensor.

Nowadays, one of the commercially available singlet oxygen sensor is "Singlet Oxygen Sensor Green™" (SOSG) from Invitrogen Corp. It is a type of reagent which after reacting with singlet oxygen emits green fluorescence while being excited at 504 nm [40]. Researchers have been trying to detect the

singlet oxygen in a cheaper way. If the quantum dots could be used as the singlet oxygen sensor, it would be a breakthrough for the cancer treatment. Various approaches of treating the cancer patients, especially photodynamic therapy could be quantitatively evaluated, given by the data from the singlet oxygen sensor.

As indicated by the user manual of the SOSG, the starting concentration should be within the range of 1~10 μM. For our experiment we used 3 mL of deionized water in the vial and in the meantime, added 200 μL 35 mM PPIX solution into the vial also. After the PPIX solution has been uniformly diluted, 20 μL SOSG (200 μM) solution were added into the vial, and shaked well then the luminescence spectra were monitored, after choosing the appropriate wavelength for excitation for both the photosensitizer and the singlet oxygen sensor.

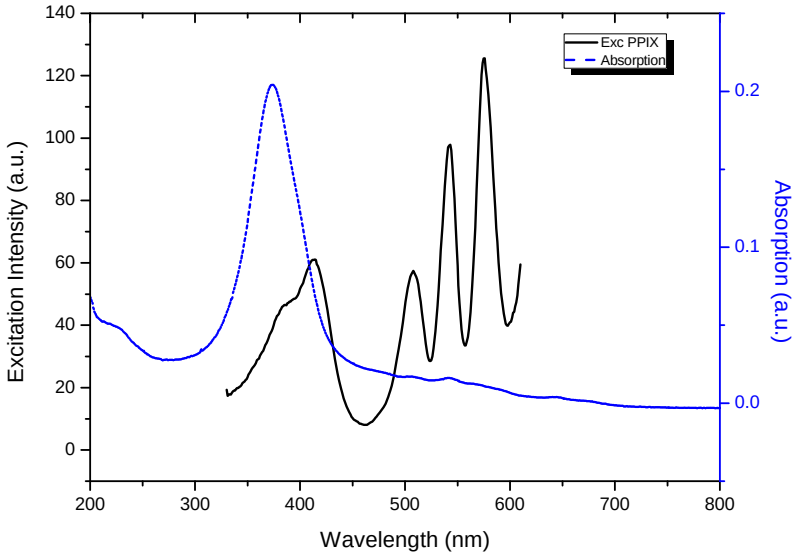

Fig 3.11 Excitation and Absorption of PPIX

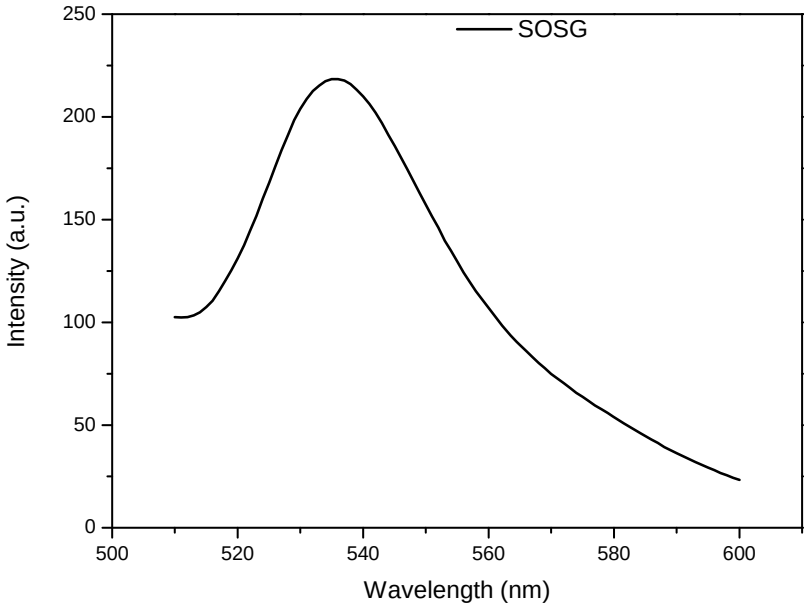

Fig 3.12 Luminescence emission spectrum of the SOSG excited at 504 nm

Fig 3.11 shows the excitation spectrum as well as the absorption spectrum of the PPIX photosensitizer. On the SOSG manual, the working excitation for SOSG is 504 nm. In the absorption spectrum of PPIX at 504 nm it is not zero and meanwhile, it is also the second peak in the excitation spectrum. (using the emission peak at 700 nm). Fig 3.12 shows the emission spectrum for the SOSG when excited at 504 nm to be at 536 nm, not like the one described in the manual as 525 nm. By using 504 nm as the excitation wavelength, we monitored the peak intensity at 536 nm as shown in Fig 3.13.

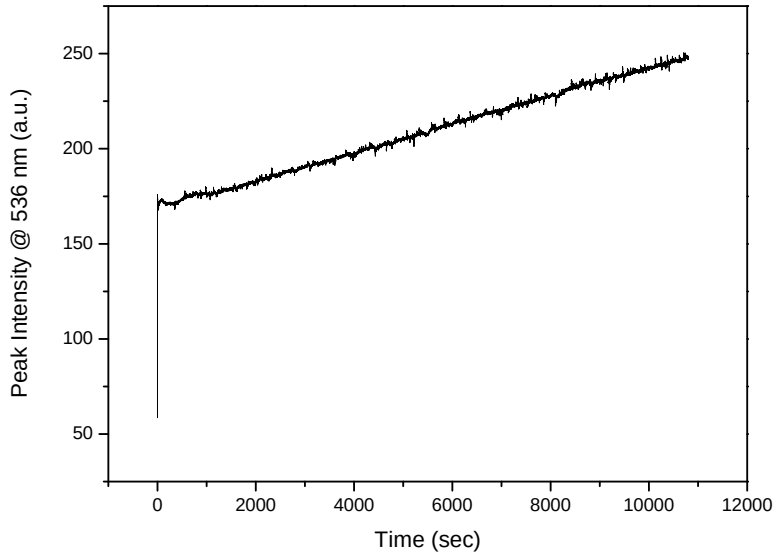

Fig 3.13 Peak intensity of SOSG at 536 nm with PPIX 200 µL (35 mM), excitation 504 nm

Even though there is some fluctuation and noise, but after taking large number of points (54000 points!), we managed to have the R square value of 0.99678 (by using Origin, linear fitting tool analysis).

Table 3.1 Summary of the linear fitting of SOSG 536 nm peak intensity versus time

	Intercept		Slope		Statistics
	Value	Std Error	Value	Std Error	Adj. R-Square
Peak Intensity	168.55703	0.01128	0.0074	1.80867E-6	0.99678

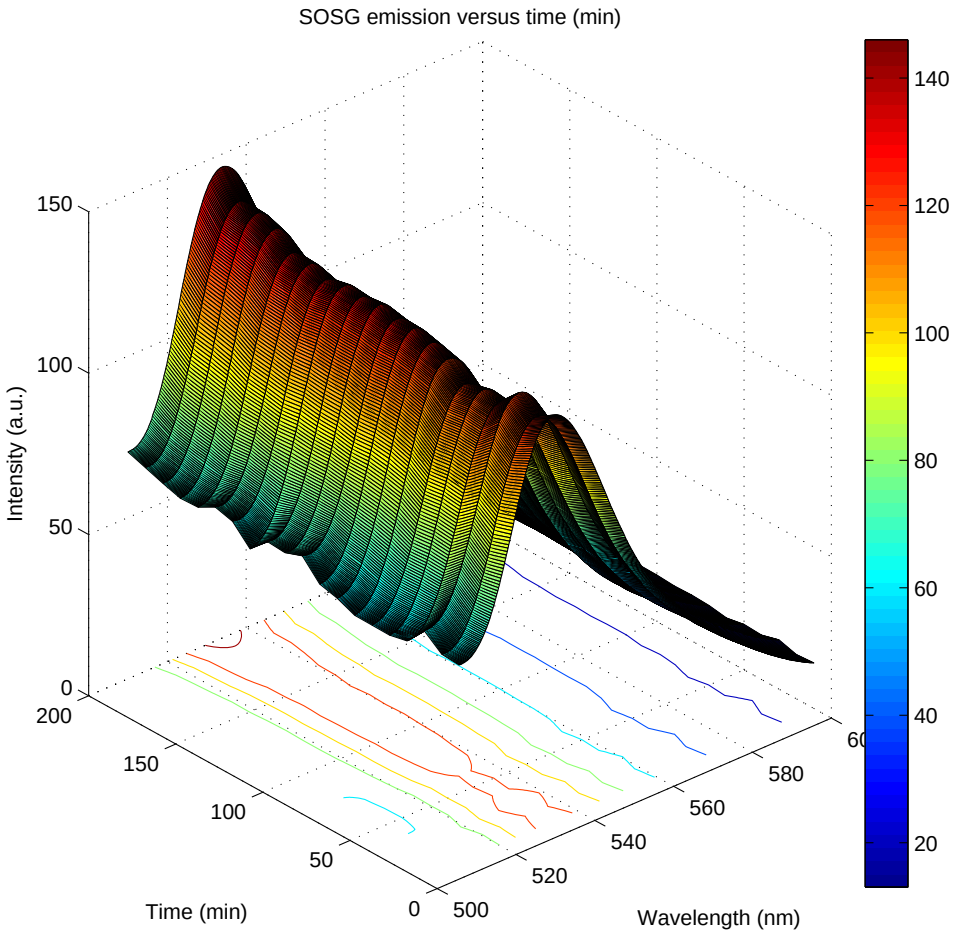

Fig 3.14 3-D illustration of the intensity of SOSG excited by 504 nm for 200 min

After being excited for 200 min with the 504 nm wavelength radiation, SOSG underwent an unstable process which happened around within the 30 min after the injection of the PPIX. It could be seen that the contour around 50 min is not smooth. Then the intensity slowly increased until it reaches 200 min to a new peak at 140. This tells us that, SOSG is still a valid singlet oxygen sensor for measuring the $^1O_2$ generated by photosensitizer PPIX even though PPIX is strongly colored. But it only gives the direct evidence of the existence of the singlet oxygen, it still cannot tell us how much singlet oxygen has been generated and how long it has survived. SOSG's luminescence response to singlet oxygen is irreversible. So its intrinsic peak intensity will continue to grow until the source of singlet oxygen has been annihilated or the ability of generating more singlet oxygen of the source has been greatly reduced. But the lifetime of singlet oxygen is relatively short, normally in micro seconds [41]. In this case,

applying SOSG's luminescence intensity directly to the concentration of the singlet oxygen is empirically hard to achieve.

Sodium azide (NaN_3) is singlet oxygen quencher. If it is added it into the PPIX solution, it is expected that the luminescence intensity increase rate to drop, or even goes to zero, with respect to time. And this is what we encountered, as shown in Fig 3.15.

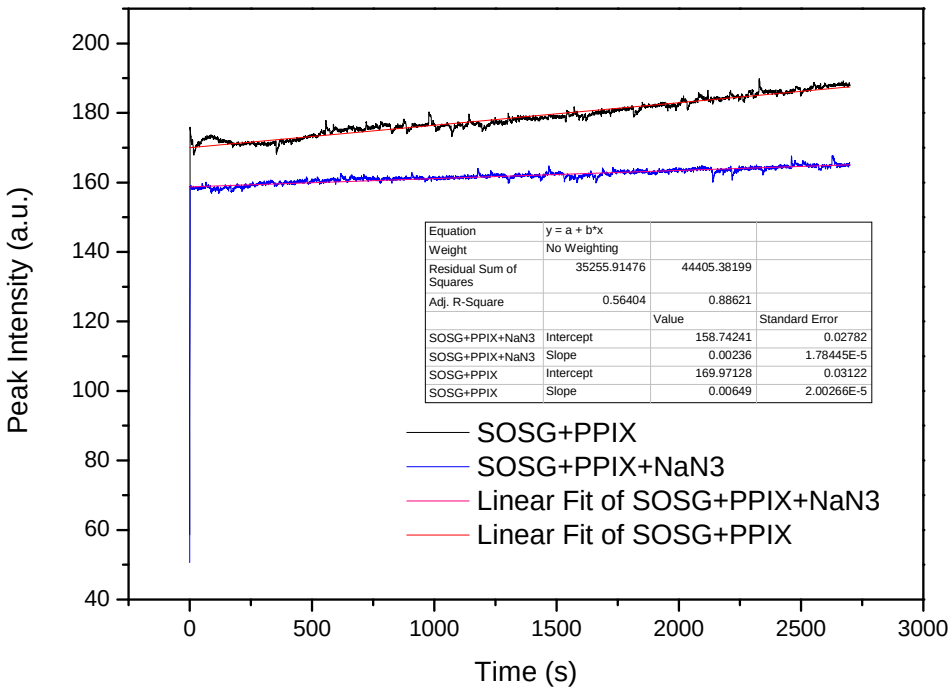

Equation	y = a + b*x		
Weight	No Weighting		
Residual Sum of Squares	35255.91476	44405.38199	
Adj. R-Square	0.56404	0.88621	
		Value	Standard Error
SOSG+PPIX+NaN3	Intercept	158.74241	0.02782
SOSG+PPIX+NaN3	Slope	0.00236	1.78445E-5
SOSG+PPIX	Intercept	169.97128	0.03122
SOSG+PPIX	Slope	0.00649	2.00266E-5

Fig 3.15 Comparison of the luminescence response of SOSG with and without NaN_3

After sodium azide to quench the luminescence, the slope goes from 0.00649 to 0.00236. (best linear fitting by Origin) The intensity also drops. The reason why the slope for the sample with sodium azide is not zero is probably because the amount of sodium azide is not enough to quench the singlet oxygen or the left over singlet oxygen has already reacted with SOSG and certain period of time is required for this process to be accomplished. After 200 min, the emission spectra of SOSG with and without NaN_3 are shown in Fig 3.16.

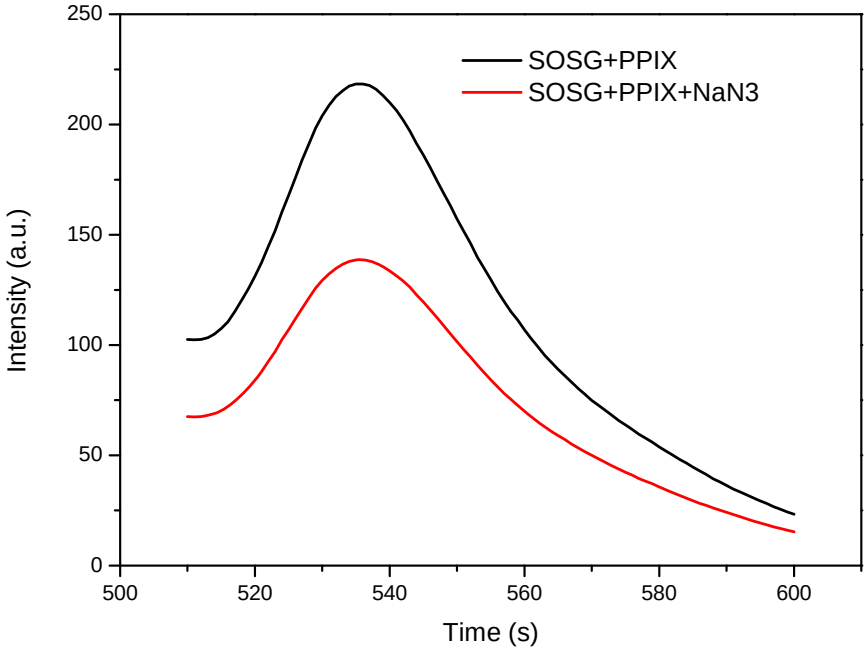

Fig 3.16 Emission spectra of SOSG with or without NaN_3 after 200 min

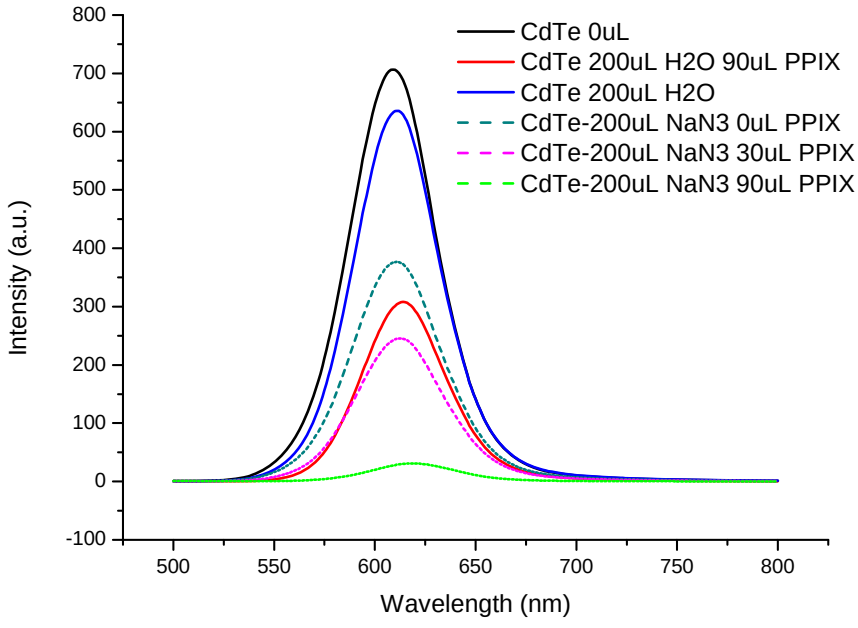

Fig 3.17 Comparison of CdTe quantum dots and the luminescence response with or without NaN_3

The same experiment using 3 mL CdTe quantum dots stabilized by CA, is shown in Fig 3.17. The black curve is the original solution without adding anything. When 200 μL deionized water was added, we have the blue curve was obtained. The red curve was obtained by adding 200 μL deionized water and 90 μL PPIX (35 mM) solution. When 200 μL sodium azide was added to the original solution, the intensity of the emission abruptly dropped to the cyan dashed line. When 30 μL and 90 μL of PPIX solution were added into the quantum dots solution mixed with NaN_3 solution, the spectrum dropped from cyan dashed line to magenta dashed line and finally to green dashed line. Here the intensity is almost zero and quantum dots has almost been quenched completely.

Since there are two different substances that have been added into the original CdTe/CA quantum dots solution, adding the sodium azide greatly decreased the luminescence, compared the one by adding the same amount of water. While adding PPIX into the same amount 90 μL, the one without sodium azide still gives luminescence but the other one with sodium azide was almost quenched. Although the reason why PPIX has the effect of decreasing the luminescence of CdTe/CA quantum dots solution is still needs to be investigated, it could be concluded that the singlet oxygen generated by the PPIX is not the "killer" for the luminescence. Or conducting this contrast experiments with or without sodium azide is not appropriate for CdTe quantum dots because whether or not singlet oxygen exists, sodium azide cannot tell us simply based on the phenomena that the luminescence will decrease one way or the other.

3.4 Conclusion

Regardless of the stabilizer used, CdTe quantum dots aqueous solution could be applied as a possible photosensitizer PPIX sensor by fitting the working curve (using the least square method) with respect to the concentration of the PPIX. But after careful investigation of the response of the quantum dots as well as contrasting it with commercially available singlet oxygen sensor SOSG, we conclude that the decrease of the luminescence of the quantum dots solution is not due to the singlet oxygen the photosensitizer generated, or sodium azide cannot be applied in evaluating the existence of the singlet oxygen within quantum dots solution. (CdTe quantum dots solution cannot be used as the singlet oxygen sensor)

CHAPTER 4

LEAD SULFIDE QUANTUM DOTS AND ITS APPLICATION IN CEA SENSING

4.1 Introduction

Semiconductor quantum dots have lots of applications. CdTe quantum dots and their derivatives are excellent examples but besides this semiconductor, there is another type of material which is lead sulfide, PbS, which has been frequently used for decades. It is a common infrared detector material, sensing photons and responding directly to radiation. So by monitoring the temperature of the material we can accurately detect the near infrared signals. It is also a unique semiconductor material, with a rather small bandgap energy (0.41 eV at 300 K); and this bandgap energy can be easily controlled by the material's scale, reaching a few electron volts when PbS particles in the nanometer scale. After this procedure, the PbS quantum dots can be customized to specific applications. Hansen et al [42] used PbS for electrochemical detection of DNA targets even the analyte amount is almost as small as untraceable. The nonradiative resonant energy transfer (NRET) also allows this type of quantum dots to be used in solar cell realm, according to Lu et al's research [43]. In this chapter, we will discuss about a simple method of synthesizing the aqueous miscible PbS quantum dots and its potential biological application. [44]

4.2 Experimental Section

The schematic setting for synthesizing PbS quantum dots is illustrated in Fig 4.1.

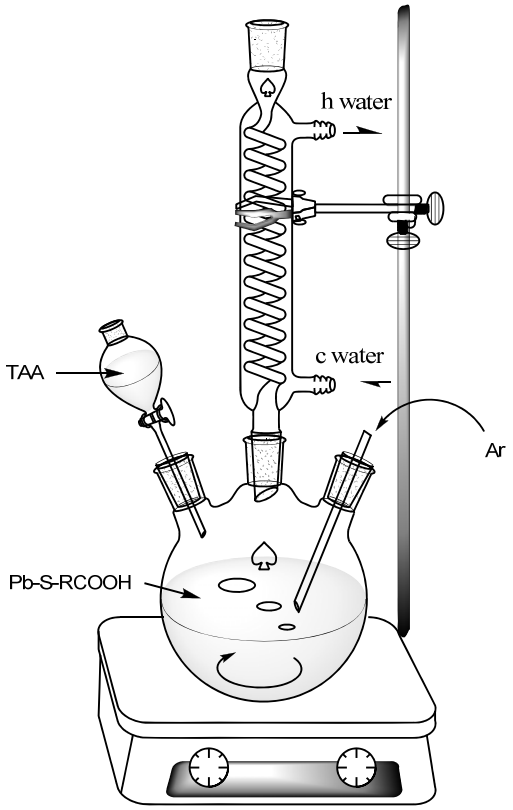

Fig 4.1 Schematic setting for synthesizing PbS quantum dots stabilized by TGA

Thioglycolic acid (TGA) stabilized PbS quantum dots were synthesized as follows. Briefly, 0.0662 g of $Pb(NO_3)_2$ (0.2 mmol) was dissolved in 100 mL of deionized water, and 0.4 mmol of TGA (approximately 0.0278 mL) were added under stirring, followed by adjusting the pH value to 11.5 by dropwise addition of 2 M solution of NaOH. The solution was placed in a three-necked flask fitted with a septum and valves and was deaerated by argon bubbling for 5 min. A thioacetamide solution, which was prepared by adding 0.2 mmol (0.015026 g) into 20 mL deionized water, was added and the solution was heated till 50 ℃. The solution was refluxed for 4 h at this temperature to promote quantum dots growth.

4.3 Characterization and Discussion

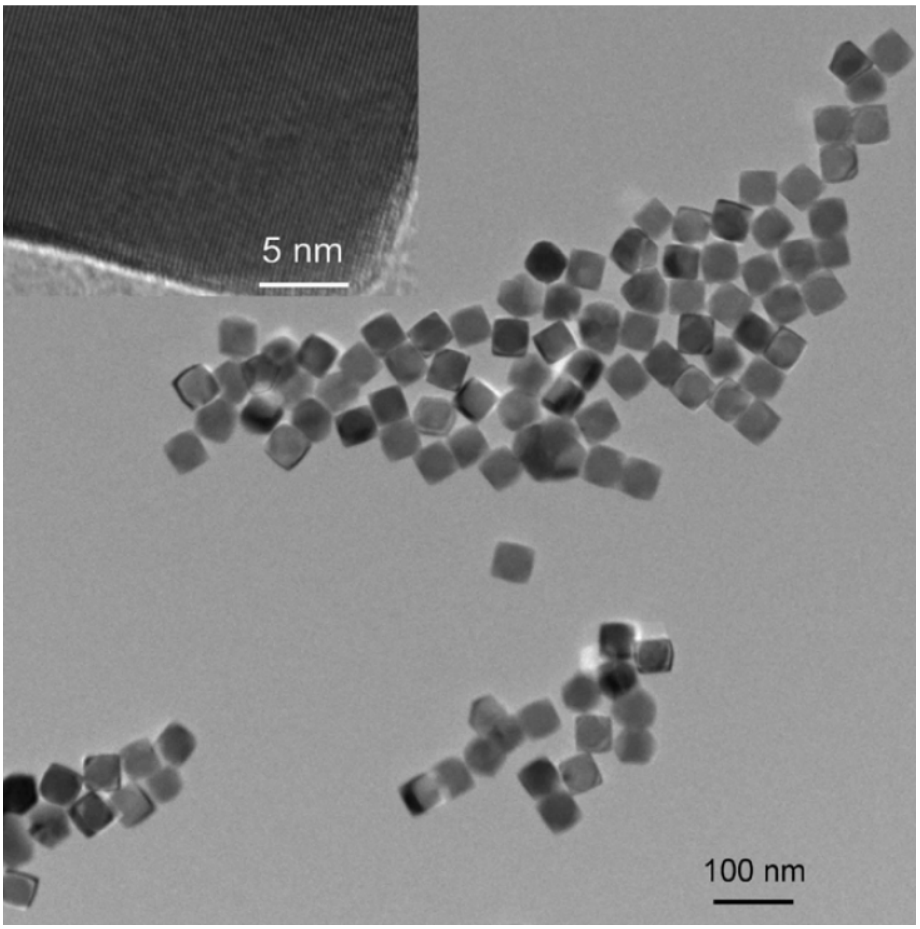

Fig 4.2 TEM image of the TGA stabilized PbS quantum dots

As seen from Fig 4.2, these high resolution TEM images were used to observe the structure, size and shape of the particles. As estimated from the TEM image the cubic PbS quantum dots are 20 nm size in average and the size distribution is very uniform. The inset of Fig 4.2 shows the high resolution TEM (HRTEM) image of one of the particles. Very clear lattice fringes can be observed here, meaning the quantum dots are highly crystallized. The lattice spacing within the inset image is 0.302nm which corresponds to the (200) planes.

A more detailed TEM image is given in Fig 4.3.

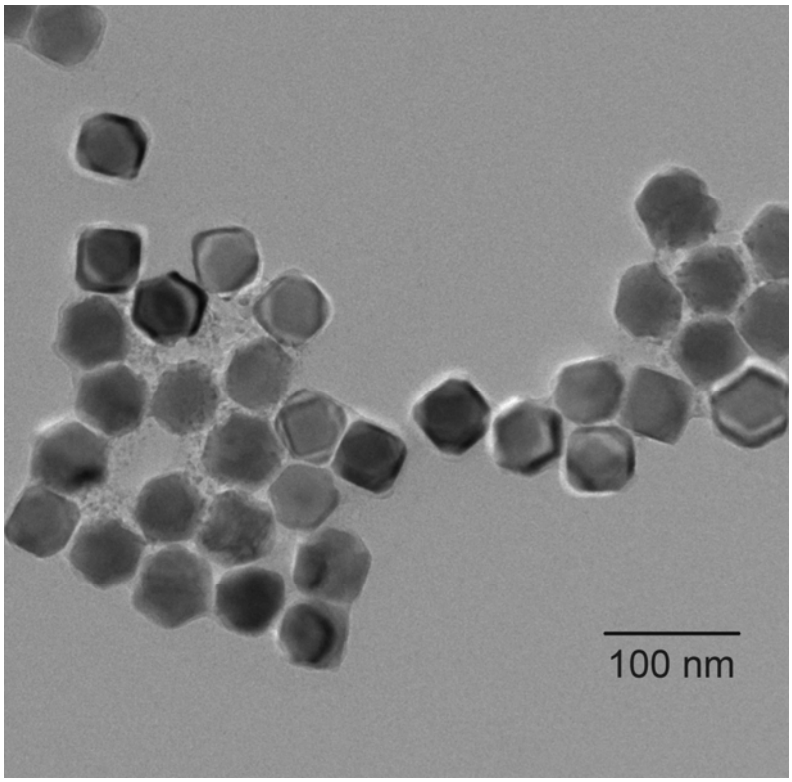

Fig 4.3 Beautifully shaped cubic PbS quantum dots, stabilized by TGA, 3 hrs reaction time

In Fig 4.3 the particles are almost uniformly distributed, giving us the average particle size to be 51.6 nm.

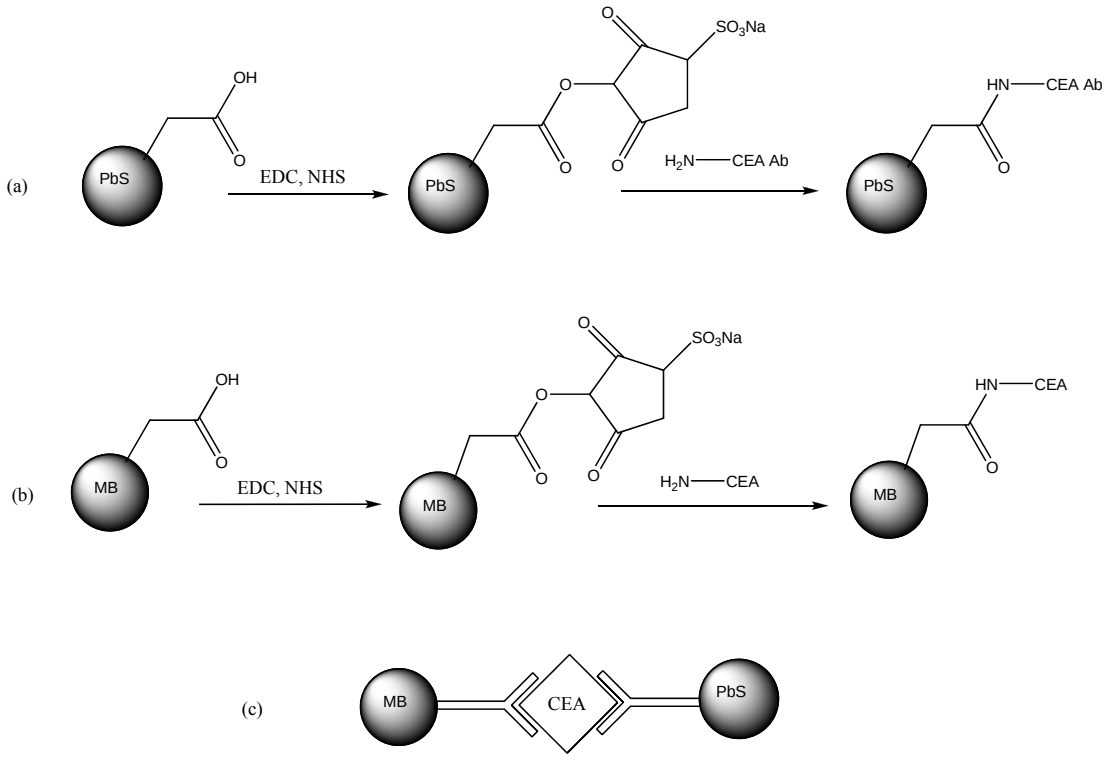

Fig 4.4 EDC&NHS bioconjugation of the (a) PbS and (b) magnetic beads
(c) The formation of the sandwich like immunocomplex for both MB as well as PbS QD

After the PbS quantum dots had been synthesized, the carcinoembyronic antigen (CEA) antibody were used to attach to the carboxylic group of the TGA in the PbS quantum dots surface using most common EDC/NHS bioconjugation approach. The commercially available magnetic beads were surface modified by carboxylic group also and were attach to CEA using the same method. Therefore, in order to use the magnetic-beads-based immunoassay both (a) and (b) would be mixed in Fig 4.4 to be able to form a sandwich structure as shown in Fig 4.4 (c).

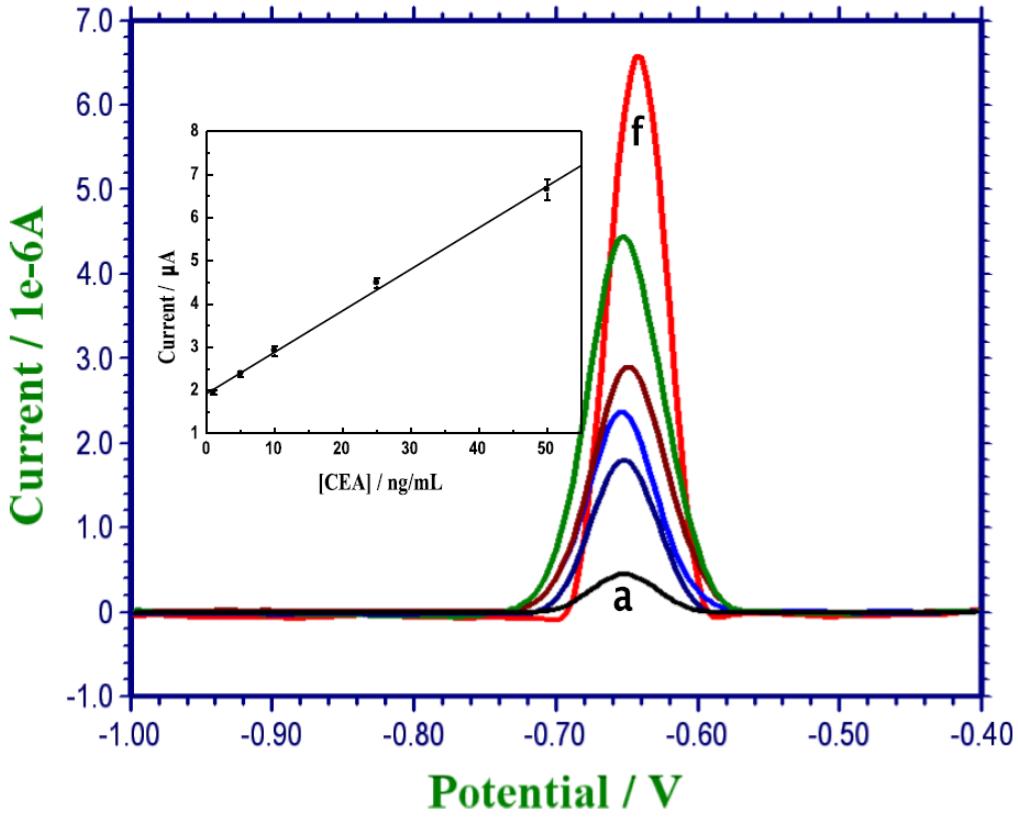

Fig 4.5 Square wave voltammograms of electrochemical immunoassay with increasing concentration of the CEA (from a to f, 0, 1.0, 5.0, 10, 25 and 50 ng mL^{-1} CEA, respectively)

The sandwich like quantum dot immunocomplex would release Pb^{2+} ions if subjected to 1 M HCl for 180s. After magnetic separation, the suspension containing the released lead ions was transferred into a centrifuge tube, and 90 μL of 0.2 M acetate buffer containing 20 μg mL^{-1} of Hg was added. The resulting solution was then transferred to a screen-printed electrode surface for square wave voltammetric (SWV) measurement. Fig 4.5 shows typical square wave voltammograms of the sandwich immunoassay with increasing concentration of CEA (0~50 ng mL^{-1}, from a to f). The resulting calibration plot of the current versus CEA (inset) is linear over the 1.0~50ng mL^{-1} range and is suitable for quantitative work.

4.4 Conclusion

Thioglycolic acid stabilized PbS quantum dots with fine shape have been synthesized by using thioacetamide as the sulfur source. The quantum dots have been used as the electrochemical immunoassay to detect the tumor biomarker CEA (cancer embryonic antigen). By coupling commercially

available magnetic beads, we take the advantage of the electrochemical stripping analysis of the Pb metal ions and CEA signal could be monitored as low as 0.5 ng mL^{-1}.

CHAPTER 5

SUMMARY AND FUTURE WORK

Recent advances in integration of quantum dots with biology and medicine have created tremendous excitement. One major reason for this trend is the rapid progress made by physical scientists in the development of synthetic recipes for manipulating and optimizing the properties of the quantum dots. Another reason is the development of chemistry to incorporate these quantum dots to biology. In our project, we managed to further optimize the parameters to tune the emission peak to near infrared region, called the near infrared window, where the brain and muscle tissue are prone to be transparent in this region so light can easily penetrate through the skin, and discussed the possible mechanism how to manipulate these parameters. Then we synthesized highly crystallized PbS quantum dots, use the voltammogram to detect the CEA signal by stripping the lead ions out of the particle. At last we managed to use the commercially available singlet oxygen sensor SOSG to measure singlet oxygen generated by the photosensitizer PPIX. After careful monitoring the experiment parameter by contrasting the singlet oxygen quencher sodium azide, we came up to the conclusion that CdTe quantum dots luminescence peak intensity could provide linear response to the photosensitizer concentration, but not the concentration of the singlet oxygen. Whether the singlet oxygen is the reason for the decrease of the luminescence intensity of the CdTe quantum dots or not, still needs to be investigated.

REFERENCES

[1] S. Santra, *et al.*, "Synthesis and characterization of fluorescent, radio-opaque, and paramagnetic silica nanoparticles for multimodal bioimaging applications," *Advanced Materials,* vol. 17, pp. 2165-2169, Sep 16 2005.

[2] S. Santra, *et al.*, "Rapid and effective labeling of brain tissue using TAT-conjugated CdS: Mn/ZnS quantum dots," *Chemical Communications,* pp. 3144-3146, 2005.

[3] H. S. Yang, *et al.*, "Gd-III-functionalized fluorescent quantum dots as multimodal imaging probes," *Advanced Materials,* vol. 18, p. 2890, Nov 3 2006.

[4] P. N. Prasad, *Nanophotonics*, 1 ed.pp. 27, Hoboken, NJ: Wiley-Interscience, 2004.

[5] A. Ross and e. a. J.B., *Topics in Fluorescence Spectroscopy* vol. 3,Tyrosine Fluorescnece and Phosphorescence from Proteins and Polypeptides, pp. 397, New York and London: Springer, 1991.

[6] L. Manna, *et al.*, "Synthesis of Soluble and Processable Rod-, Arrow-, Teardrop-, and Tetrapod-Shaped CdSe Nanocrystals," *Journal of the American Chemical Society,* vol. 122, pp. 12700-12706, 2000.

[7] A. L. Rogach, *et al.*, "Aqueous synthesis of thiol-capped CdTe nanocrystals: State-of-the-art," *Journal of Physical Chemistry C,* vol. 111, pp. 14628-14637, Oct 11 2007.

[8] P. T. Tran, *et al.*, "Use of luminescent CdSe-ZnS nanocrystal bioconjugates in quantum dot-based nanosensors," *Physica Status Solidi B-Basic Research,* vol. 229, pp. 427-432, Jan 2002.

[9] D. Gerion, *et al.*, "Synthesis and properties of biocompatible water-soluble silica-coated CdSe/ZnS semiconductor quantum dots," *Journal of Physical Chemistry B,* vol. 105, pp. 8861-8871, Sep 20 2001.

[10] W. J. Parak, *et al.*, "Conjugation of DNA to silanized colloidal semiconductor nanocrystalline quantum dots," *Chemistry of Materials,* vol. 14, pp. 2113-2119, May 2002.

[11] S. P. Wang, *et al.*, "Antigen/antibody immunocomplex from CdTe nanoparticle bioconjugates," *Nano Letters,* vol. 2, pp. 817-822, Aug 2002.

[12] X. Y. Wu, *et al.*, "Immunofluorescent labeling of cancer marker Her2 and other cellular targets with semiconductor quantum dots," *Nature Biotechnology,* vol. 21, pp. 41-46, Jan 2003.

[13] W. J. Parak, *et al.*, "Cell motility and metastatic potential studies based on quantum dot imaging of phagokinetic tracks," *Advanced Materials,* vol. 14, pp. 882-885, Jun 18 2002.

[14] B. Dubertret, *et al.*, "In vivo imaging of quantum dots encapsulated in phospholipid micelles," *Science,* vol. 298, pp. 1759-1762, Nov 29 2002.
[15] J. R. Taylor, *et al.*, "Probing specific sequences on single DNA molecules with bioconjugated fluorescent nanoparticles," *Analytical Chemistry,* vol. 72, pp. 1979-1986, May 1 2000.
[16] H. X. Xu, *et al.*, "Multiplexed SNP genotyping using the Qbead (TM) system: a quantum dot-encoded microsphere-based assay," *Nucleic Acids Research,* vol. 31, pp. -, Apr 15 2003.
[17] J. Riegler and T. Nann, "Application of luminescent nanocrystals as labels for biological molecules," *Analytical and Bioanalytical Chemistry,* vol. 379, pp. 913-919, Aug 2004.
[18] P. R. Selvin, "The renaissance of fluorescence resonance energy transfer," *Nature Structural Biology,* vol. 7, pp. 730-734, Sep 2000.
[19] T. Heyduk, "Measuring protein conformational changes by FRET/LRET," *Current Opinion in Biotechnology,* vol. 13, pp. 292-296, Aug 2002.
[20] R. N. Day, *et al.*, "Fluorescence resonance energy transfer microscopy of localized protein interactions in the living cell nucleus," *Methods,* vol. 25, pp. 4-18, Sep 2001.
[21] J. J. Li and T. D. H. Bugg, "A fluorescent analogue of UDP-N-acetylglucosamine: application for FRET assay of peptidoglycan translocase II (MurG)," *Chemical Communications,* pp. 182-183, Jan 21 2004.
[22] C. R. Kagan, *et al.*, "Electronic energy transfer in CdSe quantum dot solids," *Physical Review Letters,* vol. 76, pp. 1517-1520, Feb 26 1996.
[23] D. M. Willard, *et al.*, "CdSe-ZnS quantum dots as resonance energy transfer donors in a model protein-protein binding assay," *Nano Letters,* vol. 1, pp. 469-474, Sep 2001.
[24] D. Hesselbarth, *et al.*, "High resolution MRI and MRS: A feasibility study for the investigation of focal cerebral ischemia in mice," *Nmr in Biomedicine,* vol. 11, pp. 423-429, Dec 1998.
[25] K. Ugurbil, *et al.*, "Functional mapping in the human brain using high magnetic fields," *Philosophical Transactions of the Royal Society of London Series B-Biological Sciences,* vol. 354, pp. 1195-1213, Jul 29 1999.
[26] M. Allen, *et al.*, "Paramagnetic viral nanoparticles as potential high-relaxivity magnetic resonance contrast agents," *Magnetic Resonance in Medicine,* vol. 54, pp. 807-812, Oct 2005.
[27] M. S. Martina, *et al.*, "Generation of superparamagnetic liposomes revealed as highly efficient MRI contrast agents for in vivo imaging," *Journal of the American Chemical Society,* vol. 127, pp. 10676-10685, Aug 3 2005.
[28] R. B. Lauffer, "Paramagnetic Metal-Complexes as Water Proton Relaxation Agents for Nmr Imaging - Theory and Design," *Chemical Reviews,* vol. 87, pp. 901-927, Oct 1987.
[29] S. Rieger, *et al.*, "Quantum dots are powerful multipurpose vital labeling agents in zebrafish embryos," *Developmental Dynamics,* vol. 234, pp. 670-681, Nov 2005.
[30] A. Shavel, *et al.*, "Factors governing the quality of aqueous CdTe nanocrystals: Calculations and experiment," *Journal of Physical Chemistry B,* vol. 110, pp. 19280-19284, Oct 5 2006.

[31] A. L. Rogach, *et al.*, "Synthesis and characterization of thiol-stabilized CdTe nanocrystals," *Berichte Der Bunsen-Gesellschaft-Physical Chemistry Chemical Physics,* vol. 100, pp. 1772-1778, Nov 1996.
[32] N. Gaponik, *et al.*, "Thiol-capping of CdTe nanocrystals: An alternative to organometallic synthetic routes," *Journal of Physical Chemistry B,* vol. 106, pp. 7177-7185, Jul 25 2002.
[33] A. Rogach, *et al.*, "Colloidally prepared HgTe nanocrystals with strong room-temperature infrared luminescence," *Advanced Materials,* vol. 11, pp. 552-+, May 7 1999.
[34] M. V. Kovalenko, *et al.*, "Colloidal HgTe nanocrystals with widely tunable narrow band gap energies: From telecommunications to molecular vibrations," *Journal of the American Chemical Society,* vol. 128, pp. 3516-3517, Mar 22 2006.
[35] U. Resch, *et al.*, "Photochemistry and Radiation-Chemistry of Colloidal Semiconductors .33. Chemical-Changes and Fluorescence in Cdte and Znte," *Langmuir,* vol. 5, pp. 1015-1020, Jul-Aug 1989.
[36] S. Kim, *et al.*, "Near-infrared fluorescent type II quantum dots for sentinel lymph node mapping," *Nature Biotechnology,* vol. 22, pp. 93-97, Jan 2004.
[37] F. F. Jobsis-vanderVliet, "Discovery of the near-infrared window into the body and the early development of near-infrared spectroscopy," *Journal of Biomedical Optics,* vol. 4, pp. 392-396, Oct 1999.
[38] A. S. Susha, *et al.*, "Luminescent CdTe nanocrystals as ion probes and pH sensors in aqueous solutions," *Colloids and Surfaces a-Physicochemical and Engineering Aspects,* vol. 281, pp. 40-43, Jun 15 2006.
[39] P. Yang, *et al.*, "Formation of two types of highly luminescent SiO2 beads impregnated with multiple CdTe QDs," *New Journal of Chemistry,* vol. 33, pp. 561-567, 2009.
[40] *Singlet Oxygen Sensor Green Reagent, Manual*. Available: http://products.invitrogen.com/ivgn/product/S36002?ICID==Search-Product#
[41] B. A. Lindig, *et al.*, "Determination of the lifetime of singlet oxygen in water-d2 using 9,10-anthracenedipropionic acid, a water-soluble probe," *Journal of the American Chemical Society,* vol. 102, pp. 5590-5593, 1980.
[42] J. A. Hansen, *et al.*, "Femtomolar electrochemical detection of DNA targets using metal sulfide nanoparticles," *Journal of the American Chemical Society,* vol. 128, pp. 3860-3861, Mar 29 2006.
[43] S. Y. Lu, *et al.*, "Photocurrent Induced by Nonradiative Energy Transfer from Nanocrystal Quantum Dots to Adjacent Silicon Nanowire Conducting Channels: Toward a New Solar Cell Paradigm," *Nano Letters,* vol. 9, pp. 4548-4552, Dec 2009.
[44] S. F. Wang, *et al.*, "Electrochemical immunoassay of carcinoembryonic antigen based on a lead sulfide nanoparticle label," *Nanotechnology,* vol. 19, pp. -, Oct 29 2008.

BIOGRAPHICAL INFORMATION

Xing Zhang obtained his bachelor degree of Materials Science and Engineering in Tsinghua University, Beijing, China in July 2006. After three years of study in the Physics Department of University of Texas at Arlington, he will continue pursuing his Ph.D degree in Materials Science and Engineering in University of North Carolina at Chapel Hill, beginning of fall semester, 2010.